The Plant Cell, Vol. 23: 3463–3481, September 2011, www.plantcell.org

Multivesicular Bodies Mature from the *Trans*-Golgi Network/Early Endosome in *Arabidopsis* [W]

David Scheuring,[a,1] Corrado Viotti,[b,1] Falco Krüger,[a] Fabian Künzl,[c] Silke Sturm,[a] Julia Bubeck,[b] Stefan Hillmer,[a] Lorenzo Frigerio,[d] David G. Robinson,[a] Peter Pimpl,[a,c,2] and Karin Schumacher[b]

[a] Plant Cell Biology, Centre for Organismal Studies, University of Heidelberg, 69120 Heidelberg, Germany
[b] Developmental Biology of Plants, Centre for Organismal Studies, University of Heidelberg, 69120 Heidelberg, Germany
[c] Developmental Genetics, Centre for Plant Molecular Biology, University of Tübingen, 72076 Tuebingen, Germany
[d] Department of Biological Sciences, University of Warwick, Coventry CV4 7AL, United Kingdom

The plant *trans*-Golgi network/early endosome (TGN/EE) is a major hub for secretory and endocytic trafficking with complex molecular mechanisms controlling sorting and transport of cargo. Vacuolar transport from the TGN/EE to multivesicular bodies/late endosomes (MVBs/LEs) is assumed to occur via clathrin-coated vesicles, although direct proof for their participation is missing. Here, we present evidence that post-TGN transport toward lytic vacuoles occurs independently of clathrin and that MVBs/LEs are derived from the TGN/EE through maturation. We show that the V-ATPase inhibitor concanamycin A significantly reduces the number of MVBs and causes TGN and MVB markers to colocalize in *Arabidopsis thaliana* roots. Ultrastructural analysis reveals the formation of MVBs from the TGN/EE and their fusion with the vacuole. The localization of the ESCRT components VPS28, VPS22, and VPS2 at the TGN/EE and MVBs/LEs indicates that the formation of intraluminal vesicles starts already at the TGN/EE. Accordingly, a dominant-negative mutant of VPS2 causes TGN and MVB markers to colocalize and blocks vacuolar transport. RNA interference–mediated knockdown of the annexin ANNAT3 also yields the same phenotype. Together, these data indicate that MVBs originate from the TGN/EE in a process that requires the action of ESCRT for the formation of intraluminal vesicles and annexins for the final step of releasing MVBs as a transport carrier to the vacuole.

INTRODUCTION

The endomembrane system of eukaryotic cells provides the spatial and temporal separation required for the sequence of steps involved in protein trafficking. The flux of membranes and cargo through the post-Golgi compartments is enormous, and although substantial progress has been made in the identification of the different endosomal compartments in plants, we know very little about their biogenesis and their highly dynamic spatiotemporal relationships. In mammalian cells, endocytic cargo proteins are first delivered to early endosomes (EEs) (van Meel and Klumperman, 2008; Jovic et al., 2010), compartments that typically have two structurally distinct domains: a central more-or-less spherical structure with a few 50-nm-diameter intraluminal vesicles (ILVs) and an extensive network of tubules projecting outwardly into the cytoplasm (Griffiths and Gruenberg, 1991; Tooze and Hollinshead, 1991). The tubular extensions of the EE bear clathrin-coated buds (Stoorvogel et al., 1996), which are positive for the two adaptor complexes AP-1 and AP-3 (Peden et al., 2004). The small (sorting nexins 1 and 2) and large subunits of retromer are also present on these tubules (Carlton et al., 2005; Mari et al., 2008). According to Mari et al. (2008), EEs in mammalian cells are defined as compartments accessible to internalized transferrin and have one to eight ILVs. By contrast, the late endosome (LE) is more or less spherical, contains at least nine ILVs and is devoid of transferrin.

Endocytosed cargo destined for degradation becomes ubiquitinated at the plasma membrane (PM), and this signal causes them to be sorted into the ILV (Polo et al., 2002). This step, which effectively segregates ligand-receptor complexes from the cytoplasm, is critical for the cessation of signaling cascades that continue even after internalization of the receptor-ligand complex (Taub et al., 2007). Sorting into the ILV involves recognition of the ubiquitin tag by the first of four ESCRT complexes that associate with the surface of the endosomal membrane. ESCRT-0 associates with the membrane of the endosome through an interaction of the FYVE (named after the four Cys-rich proteins: Fab1, YOTB, Vac1, and EEA1) domain of HRS (hepatocyte growth factor–regulated Tyr-kinase substrate) with phosphatidylinositol 3-phosphate. It sequesters ubiquitinated cargo molecules into double-layered clathrin microdomains (Clague, 2002). These domains are visible at the surface of both EEs and LEs (Sachse et al., 2002; Murk et al., 2003). ESCRT-I and -II complexes then deform the limiting membrane into inwardly directed buds and recruit the ESCRT-0 + attached ubiquitinated cargo into the necks of the buds. ESCRT-III, in collaboration with a deubiquitinating enzyme (Doa4), then releases the ubiquitin and causes a scission of the

[1] These authors contributed equally to this work.
[2] Address correspondence to peter.pimpl@zmbp.uni-tuebingen.de.
The author responsible for distribution of materials integral to the findings presented in this article in accordance with the policy described in the Instructions for Authors (www.plantcell.org) is: Peter Pimpl (peter.pimpl@zmbp.uni-tuebingen.de).
[W] Online version contains Web-only data.
www.plantcell.org/cgi/doi/10.1105/tpc.111.086918

buds (Wollert and Hurley, 2010). Finally, the activity of an AAA-ATPase (Vps4) leads to dissociation of the ESCRT complexes. Delivery of the ILVs to the lysosome interior then occurs by fusion of the LE with the lysosome (Luzio et al., 2009).

In mammalian cells, it is generally regarded that the movement of molecules along the biosynthetic-endocytic pathways to the lysosome is accompanied by a maturation of endosomal organelles. Many of the key factors in this process have now been identified. In addition to the ESCRT complexes, both COPI (Aniento et al., 1996; Gabriely et al., 2007; Razi et al., 2009) and annexin A2 are specifically required (Mayran et al., 2003; Futter and White, 2007; Morel and Gruenberg, 2009). Also critical for the transition from EE to LE is the protein SAND-1/Mon1, which appears to be responsible for the exchange of Rab GTPases, from Rab5 (EE) to Rab 7 (LE) (Poteryaev et al., 2010).

The organelles of the plant endocytic pathway have both similarities and differences to those present in mammalian cells. Perhaps the greatest similarity lies in the morphology of the LE, occasionally termed the prevacuolar compartment in the plant literature (Lam et al., 2007; Miao et al., 2008). This is spherical, contains ILVs, and also bears a plaque on its surface and is often named a multivesicular body (MVB) (Tse et al., 2004; Otegui and Spitzer, 2008; Viotti et al., 2010). However, unlike the situation in animal cells, several studies have shown that higher plants do not have separate *trans*-Golgi network (TGN) and EE compartments (Dettmer et al., 2006; Lam et al., 2007; Reichardt et al., 2007; Otegui and Spitzer, 2008; Robinson et al., 2008; Toyooka et al., 2009; Viotti et al., 2010). The TGN in plants appears to be synonymous with the partially coated reticulum (Pesacreta and Lucas, 1984; Hillmer et al., 1988; Tanchak et al., 1988) and is a tubular-vesicular structure bearing clathrin-coated vesicles (CCVs) (Kang and Staehelin, 2008; Toyooka et al., 2009). The recent demonstration that plant retromer is present at the TGN rather than the MVB (Niemes et al., 2010b) is therefore in agreement with the location of this recycling coat complex to the tubular extensions of the EE in mammalian cells. Thus, at the morphological level, the higher plant TGN shares many features with the mammalian EE.

Based on studies with the brassinosteroid receptor BRI1, it has been established that plants also show endosomal-based signaling that appears to cease when the receptor reaches the LE (Geldner et al., 2007). Plants also possess ESCRT proteins (Winter and Hauser, 2006; Schellmann and Pimpl, 2009; Shahriari et al., 2011), but there are no clear homologs to the ESCRT-0 complex (Leung et al., 2008), and the exact location of the other complexes is unclear. Nevertheless, several studies with mutated ESCRT proteins point to their presence at least at the LE. Expression of a mutant form of Vps4 (SKD1) leads to the missorting of vacuolar proteins (Shahriari et al., 2010) as well as to an enlargement of MVBs with fewer ILVs (Haas et al., 2007). A reduction in number of ILVs and a displacement of cargo molecules destined for vacuolar degradation to the boundary membrane of the MVB was also observed after expression of mutated forms of the ESCRT-associated CHMP1A/B proteins (Spitzer et al., 2009).

In this article, we present evidence that in plants the MVB/LE is derived from the TGN/EE through a process of maturation and finally mediates vacuolar delivery by fusing with the tonoplast. Proceeding from our previous observation that vacuolar sorting receptors (VSRs) recycle from the TGN and thus do not contribute to post-TGN transport of soluble vacuolar proteins (Niemes et al., 2010a), we now show that inhibition of clathrin-mediated transport does not prevent the arrival of soluble cargo molecules, carrying vacuolar sorting determinants, in the vacuole. This raises questions about the mechanism of TGN to MVB/LE transport. Based on the observation that the V-ATPase inhibitor concanamycin A (ConcA) causes the incorporation of TGN proteins into the Golgi stack in *Arabidopsis thaliana* root cells (Viotti et al., 2010), we now show that this treatment also leads to a drastic reduction in MVB numbers. We have been able to capture the moment of MVB formation at the TGN, an event that can also be observed during the recovery of the Golgi apparatus upon ConcA washout. These data are supported by a series of experiments in which the separation of signals for fluorescent TGN and MVB marker proteins was prevented by ConcA and a dominant-negative mutant of ESCRT-III as well as the knockdown of the *Arabidopsis* annexin ANNAT3. Moreover, we show that ESCRT-I, -II, and -III are differentially distributed between TGN and MVB and that ESCRT-III is required for vacuolar transport.

RESULTS

GFP-Hub1 Inhibits Endocytosis but Not Transport to the Lytic Vacuole

We wanted to investigate whether CCVs contribute to the delivery of soluble cargo molecules to the vacuole. The expression of the C-terminal third of the clathrin heavy chain, also known as the clathrin hub, inhibits CCV formation and, thus, clathrin-mediated transport events (Liu et al., 1995, 1998; Dhonukshe et al., 2007). It was recently shown that expression of a fluorescently tagged clathrin hub (green fluorescent protein [GFP]-Hub1) in *Arabidopsis* protoplasts inhibits the endocytic uptake of the amphiphilic styryl dye FM4-64 (Dhonukshe et al., 2007). We have now used this inhibitory effect on FM4-64 uptake as a positive control for the inhibition of clathrin-mediated trafficking. In control protoplasts, the dye stained the PM instantly after addition (Figure 1A), and internalized signals were detectable 30 min later (Figure 1B). When GFP-Hub1 was expressed, an inhibition of FM4-64 uptake was observed (Figure 1C). To quantify this effect, we counted and compared the number of internal FM4-64 signals in protoplasts in the presence and absence of GFP-Hub1. For this, 20 protoplasts showing an observable amount of cytoplasm were considered. In control protoplasts, the number of internal FM4-64 signals was 37 ± 12, but the number of signals in protoplasts expressing GFP-Hub1 dropped to 7 ± 3 (Figure 1D). To test whether clathrin is required for transport to the lytic vacuole, we performed coexpression experiments of GFP-Hub1 with the soluble, vacuolar reporter signal peptide-red fluorescent protein-alanine phenylalanine valine tyrosine (spRFP-AFVY) (Hunter et al., 2007). This reporter is efficiently transported to the vacuole, even if coexpressed with fluorescent cytosolic proteins (cytGFP; Figure 1E). The expression of GFP-Hub1 does not change the intensity of the vacuolar signal pattern of spRFP-AFVY (Figure 1F), indicating that the reporter still reaches the lumen of the vacuole under these conditions.

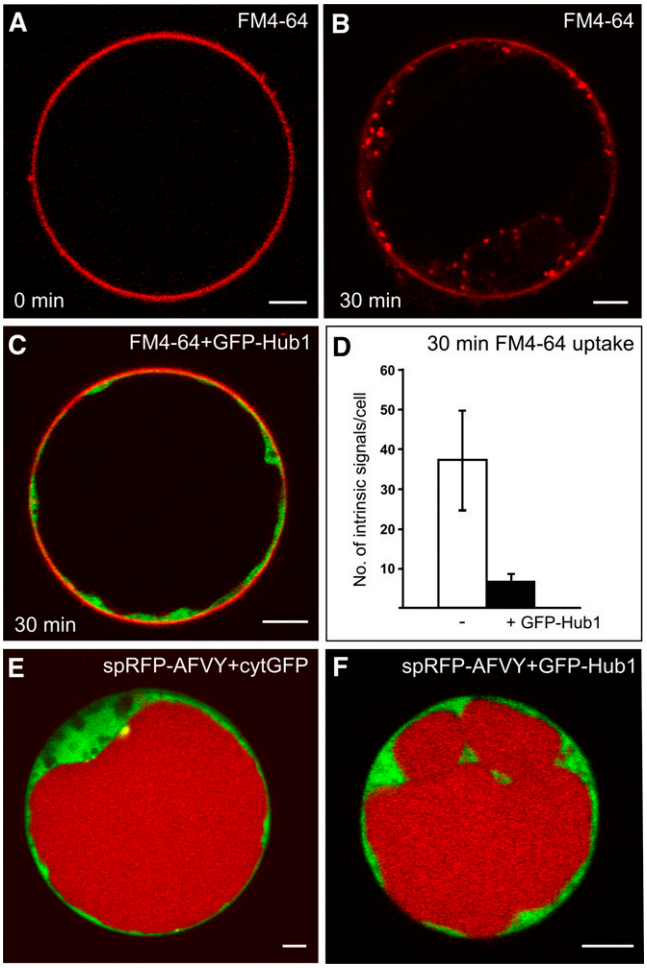

Figure 1. Clathrin-Hub1 Expression Inhibits Endocytosis but Not Vacuolar Transport in *Arabidopsis* Protoplasts.

(A) and **(B)** Staining of the PM directly after FM4-64 addition **(A)** and endocytic uptake of the dye after 30 min incubation **(B)**.

(C) Protoplasts expressing the GFP-tagged clathrin-Hub1 (GFP-Hub1) were stained with FM4-64 and incubated for 30 min. The dye is not internalized and remains at the PM.

(D) Comparative quantification of intrinsic FM4-64 signals from 20 protoplasts either in the presence or absence of GFP-Hub1. Error bars indicate the SD of signal numbers.

(E) Coexpression of the soluble vacuolar marker spRFP-AFVY and cytosolic GFP (cytGFP) in protoplasts. spRFP-AFVY is efficiently transported into the lumen of the vacuole, even if fluorescent cytosolic proteins (cytGFP) are coexpressed.

(F) Coexpression of GFP-Hub1 and the soluble vacuolar marker spRFP-AFVY in protoplasts. The presence of GFP-Hub1 in the cytosol does not perturb vacuolar transport of spRFP-AFVY (cf. to **[E]**).

Bars = 5 μm.

V-ATPase Activity Is Required for MVB Biogenesis

To examine the function of the TGN for vacuolar transport, we analyzed the effect of the V-ATPase inhibitor ConcA. Transmission electron microscopy (TEM) analysis revealed that the number of MVBs decreased significantly upon ConcA treatment. In 100 sectioned cells, the number of MVBs was 220 ± 30, whereas it was approximately fivefold lower (40 ± 15) after ConcA treatment (Figure 2A). We have shown previously that ConcA leads to morphological changes of both the Golgi apparatus and the TGN and causes intrinsic TGN membrane proteins to locate to the Golgi stack (Viotti et al., 2010). We thus decided to investigate the behavior of MVB markers upon ConcA treatment using immunogold electron microscopy (IEM). In *Arabidopsis* roots, the endogenous VSR BP80 localizes to both the TGN and the MVB (Figure 2C) (Niemes et al., 2010b; Stierhof and El Kasmi, 2010; Viotti et al., 2010), while upon ConcA treatment, BP80 locates mainly to the Golgi stack (Figures 2B, 2D, and 2E). The same result was obtained with the Rab GTPase ARA7, which in untreated cells is localized on the limiting membrane of MVBs (Figure 2F) (Haas et al., 2007; Robinson et al., 2008), while it locates to the Golgi stack in ConcA-treated cells (Figures 2B and 2G). Interestingly, both BP80 and ARA7 are still detectable at the limiting membrane of the remaining MVBs after ConcA treatment (Figures 2E and 2G). These data have been confirmed by confocal laser scanning microscopy (CLSM) analysis of transgenic *Arabidopsis* seedlings expressing the TGN marker VHA-a1-GFP and the MVB marker mRFP-ARA7. To quantify colocalization results, we calculated the linear Pearson (r_p) and the nonlinear Spearman's rank (r_s) correlation coefficient (PSC) for the pixels representing the fluorescence signals in both channels. Levels of colocalization can range from +1 for positive correlation to −1 for negative correlation (French et al., 2008). The fluorescence values of pixels across the two channels were additionally depicted in an intensity scatterplot. In untreated cells, the VHA-a1-GFP and mRFP-ARA7 signals were mostly separate (see Supplemental Figures 1A and 1B online; $r_p = 0.22$ and $r_s = 0.19$), but colocalization increased upon 30 min ConcA treatment (see Supplemental Figures 1C and 1D online, $r_p = 0.45$ and $r_s = 0.43$). Together, these findings show that V-ATPase activity is required not only for the functionality of the TGN but also for the occurrence of MVBs.

Perturbation of TGN function by ConcA inhibits protein export from the TGN but also reduces the overall number of MVBs per cell. This suggests that MVBs that once existed can disappear if the vacuolar transport route is perturbed at this step. One explanation for this could be that they are consumed in the process of vacuolar transport by fusion with the vacuole. The analysis of untreated high-pressure frozen *Arabidopsis* root cells confirmed that MVBs indeed fuse with the tonoplast to deliver their content into the vacuolar lumen (Figures 3A to 3D).

We then used TEM to investigate the origin of MVBs. Mature MVBs have an almost spherical shape (Figures 4A and 4B). TEM analysis of high-pressure frozen *Arabidopsis* root cells revealed nascent MVBs still being connected to tubular structures, indicating their TGN-based biogenesis (Figures 4C and 4D). However, after ConcA treatment followed by a short recovery period in the absence of the inhibitor, we detected multiple examples of MVBs of unusual size and form, often with bottleneck terminations, indicating that they are still connected to tubular structures of the TGN (Figures 4E to 4H). A clear connection between nascent MVBs and TGN-like structures is shown in Figures 4I and 4K. Finally, we tested the identity of these multivesiculated compartments with IEM of mRFP-ARA7 in ConcA-treated cells.

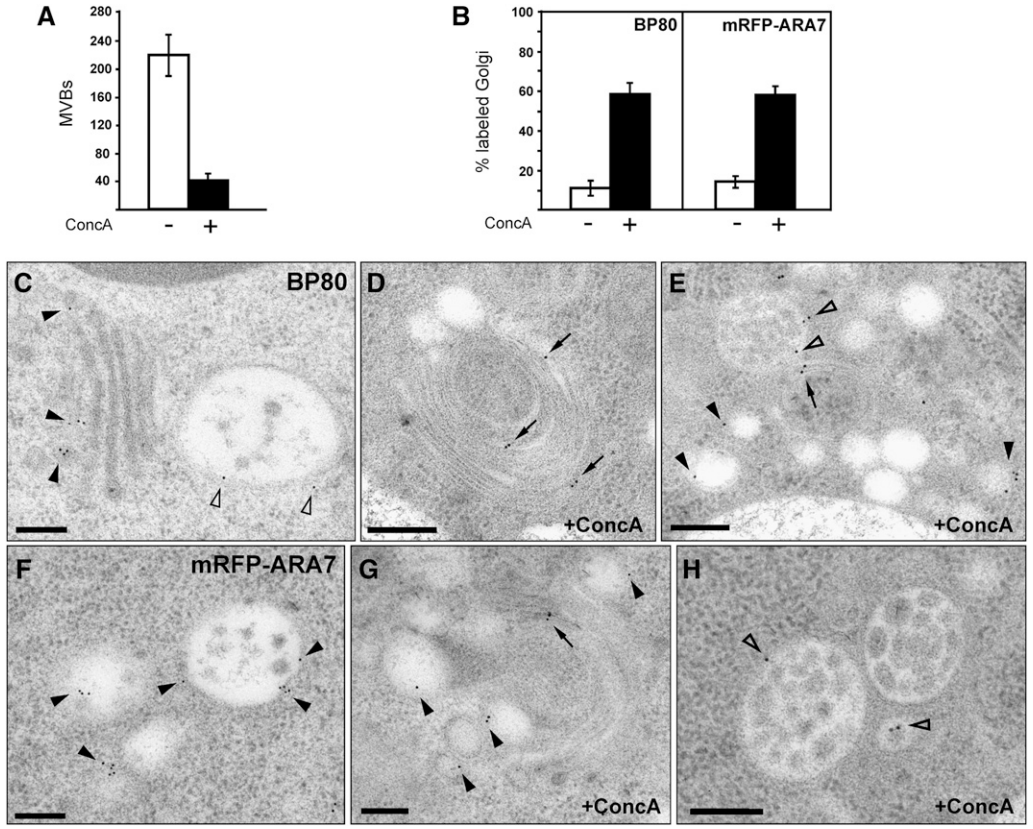

Figure 2. EM Analysis of the Effects of ConcA on MVBs.

(A) ConcA treatment reduces the number of MVBs in the cell. Roots of four independent plants were analyzed either in the absence or presence of ConcA by counting the number of MVBs in 100 sectioned cells per root. Per 100 control cells, 220 ± 30 MVBs were identified, whereas after ConcA treatment, the number of MVBs was fivefold lower (40 ± 15). Error bars indicate the SD.

(B) Quantitative analysis of ConcA effects on the endogenous VSR BP80 and the Rab GTPase ARA7 in an mRFP-ARA7–expressing *Arabidopsis* line. The Golgi localization of BP80 and mRFP-ARA7 was analyzed in roots of four independent plants either in the absence or presence of ConcA by counting the labeling on 50 randomly chosen Golgi stacks per root. Under standard conditions, BP80 and mRFP-ARA7 do not localize to the Golgi (11% ± 4% and 15% ± 2% of Golgi labeling, respectively), whereas in the presence of ConcA, both proteins also significantly localize to the Golgi stacks (59% ± 5% and 58% ± 4% of Golgi labeling, respectively). Error bars indicate the SD.

(C) IEM localization of the endogenous BP80 in *Arabidopsis* roots after high-pressure freezing, freeze substitution and Lowicryl HM20 resin embedding. The VSR BP80 localizes to both the TGN (closed arrowheads) and MVBs (open arrowheads).

(D) and **(E)** Upon ConcA treatment, BP80 is detected at the Golgi stack (**[D]**; arrows) and at enlarged vesicles in the surrounding area (**[E]**; closed arrowheads). Although ConcA reduces the number of MVBs, those MVBs that are still present show unaltered BP80 labeling (**[E]**; open arrowheads).

(F) The Rab GTPase mRFP-ARA7 localizes to the limiting membrane of MVBs (arrowheads).

(G) After ConcA treatment, mRFP-ARA7 localizes to both swollen vesicles (arrowheads) and the Golgi stack (arrows).

(H) In the presence of ConcA, mRFP-ARA7 is detected at the limiting membrane of the remaining MVBs (open arrowheads).

Bars = 200 nm

Indeed, we were able to detect ARA7 at the limiting membrane of MVBs displaying bottleneck terminations (Figure 4K).

The ESCRT Components VPS28, VPS22, and VPS2 Are Differentially Distributed between the TGN/EE and the MVB/LE

If MVBs are indeed derived from the TGN/EE via maturation, it has to be assumed that the ESCRT-mediated formation of ILVs starts already at the TGN/EE. Therefore, we examined the subcellular distribution of the ESCRT machinery.

We generated antibodies against VPS28-1 (one of the two *Arabidopsis* VPS28 isoforms, hereafter referred to as VPS28), a subunit of ESCRT-I, the potentially initiating complex in plants. To determine the specificity of the antiserum, we performed immunoblot analysis on total extracts from 7-d-old *Arabidopsis* plants and expressed a fluorescent fusion of VPS28 (VPS28-GFP) in protoplasts derived from suspension cultivated *Arabidopsis* cells. The antibody recognizes an endogenous protein in the total extracts, which correlates well with the calculated molecular mass of 23.5 kD for VPS28, and an ~50 kD protein, representing VPS28-GFP (Figure 5A). IEM of the endogenous

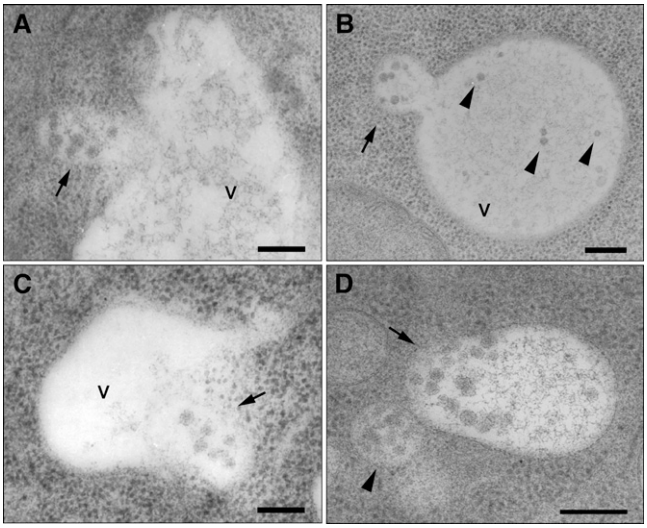

Figure 3. MVBs Fuse with the Vacuole.

Fusion of MVBs with the vacuole in sections of cells from high-pressure frozen *Arabidopsis* roots. V, vacuole; Bars = 200 nm

(A) and **(B)** The limiting membrane of an MVB (arrow) has fused with the tonoplast, resulting in the merge of the lumen of both compartments. In **(B)**, internal vesicles are recognizable in the lumen of the vacuole (arrowheads), sharing shape and size with ILVs, typically seen in MVBs (courtesy of York-Dieter Stierhof).

(C) An MVB (arrow) almost entirely fused with a small vacuole.

(D) An MVB (arrow), entirely fused with a small vacuole, shows a polarized distribution of the inner vesicles, suggesting that the fusion occurred shortly before freezing of the cells. Note that there is another MVB in the vicinity (arrowhead).

VPS28 using high-pressure frozen and freeze-substituted roots from *Arabidopsis* revealed a specific labeling of the TGN and the Golgi, but not the MVB (Figures 5B to 5D for the quantitative analysis). The unexpected TGN localization of VPS28 was confirmed by immunocolocalization in an *Arabidopsis* line, expressing a TGN marker (SYP61-CFP) under the control of the endogenous promoter (Figure 5E) and the detection of VPS28 in the core of the brefeldin A (BFA)–induced compartment in root cells of wild-type *Arabidopsis* plants (Figure 5F).

To determine the localization of other putative ESCRT complexes, we analyzed VPS22, representing ESCRT-II, and VPS2.1 (one of the three *Arabidopsis* VPS2 isoforms, hereafter referred to as VPS2), representing ESCRT-III, in coexpression studies with marker proteins for different compartments in tobacco (*Nicotiana tabacum*) protoplasts.

Coexpression of VPS22-GFP with the TGN/EE marker yellow fluorescent protein (YFP)-SYP61 reveals significantly higher values of the PSC coefficients than VPS22-GFP coexpressed with the MVB/LE marker mRFP-VSR2 (Figures 6A to 6C; see Supplemental Figures 2A to 2D online), indicating that the ESCRT-II component mainly localizes to the TGN/EE. By contrast, the values of the PSC coefficients of VPS2-GFP and YFP-SYP61 are lower than for VPS2-GFP coexpressed with the MVB/LE marker mRFP-VSR2 (Figures 6D to 6F; see Supplemental Figures 2E to 2H online).

Both VPS22-GFP and VPS2-GFP, when coexpressed with the Golgi marker Man1-RFP, have very low or even negative r_p and r_s values (see Supplemental Figures 3A to 3F online). Immunolabeling using VPS2 antibodies also confirmed that endogenous VPS2 is not present at the Golgi stack but partially localizes to the MVB/LE (see Supplemental Figures 3J to 3L online). In agreement with the differential distribution of VPS22-GFP and VPS2-GFP, coexpression of these two ESCRT components resulted in PSC coefficients of $r_p = 0.61$ and $r_s = 0.20$ (Figures 6G and 6I; see Supplemental Figures 2I and 2J online). Treatment with wortmannin (WM) showed that only VPS2-RFP signals, but not VPS22-GFP signals, were sensitive to WM, judged by the appearance of typical ring-like structures (magnified inset, Figure 6G). The number of VPS2-RFP signals exceeded that of VPS22-GFP (21.5 ± 5.5 for VPS2-RFP and 12.2 ± 3.4 for VPS22-GFP; Figure 6H). It is therefore likely that VPS22-GFP and VPS2-RFP colocalize at the TGN/EE but not at the MVB/LE. However, due to the cytosolic nature and the resulting background of the analyzed fluorescent ESCRT proteins, all of the r_p and r_s values are relatively low. Even if fusions of VPS2 with different fluorescent proteins are coexpressed, the values for the PSC coefficients do not exceed $r_p = 0.66$ and $r_s = 0.44$ (VPS2-GFP and VPS2-RFP; see Supplemental Figures 3G and 3I online). These combined findings indicate that the ESCRT-II component VPS22 and the ESCRT-III component VPS2 are gradually distributed along the vacuolar route.

VPS2-DN and Treatment with ConcA Prevent the Arrival of Soluble Reporter Molecules in the Vacuole

We next asked whether ESCRT function is required for vacuolar transport. To answer this, we used a dominant-negative VPS2 mutant (VPS2-DN), which was generated by deleting the C-terminal MIT-interacting motif responsible for the interaction with SKD1 (Obita et al., 2007; Hurley and Yang, 2008). Vacuolar transport of the reporter α-amylase-sporamin (amy-spo) was measured as the secretion index (SI) given by the ratio of amy-spo detected in the culture medium and within the cells (Pimpl et al., 2003). Coexpression of VPS2-DN caused dosage-dependent-induced secretion of amy-spo, indicating that vacuolar transport was blocked (Figure 7A). A comparable dosage-dependent misrouting of vacuolar cargo was also caused by ConcA treatment (Figure 7B). To biochemically compare the effects of VPS2-DN and ConcA, we used protein gel blots and analyzed the processing of the soluble cargo GFP-sporamin in the vacuole. Only a faint GFP-sporamin signal was detected in the medium, whereas two strong bands corresponding to GFP-sporamin and the processed form of GFP (vacuolar form) were detectable in the cell fraction (Figure 7C). Treatment with 0.3 μM ConcA showed an increase of the signal detected in the medium, and increasing concentrations of VPS2-DN also showed increasing signal strength in the medium together with a loss of the vacuolar form of GFP in the cells (Figure 7C).

VPS2-DN Induces Increased Colocalization of TGN/EE and MVB/LE Markers

Since VPS2-DN affects vacuolar transport, we analyzed its effects on the localization of YFP-SYP61 and mRFP-VSR2 as

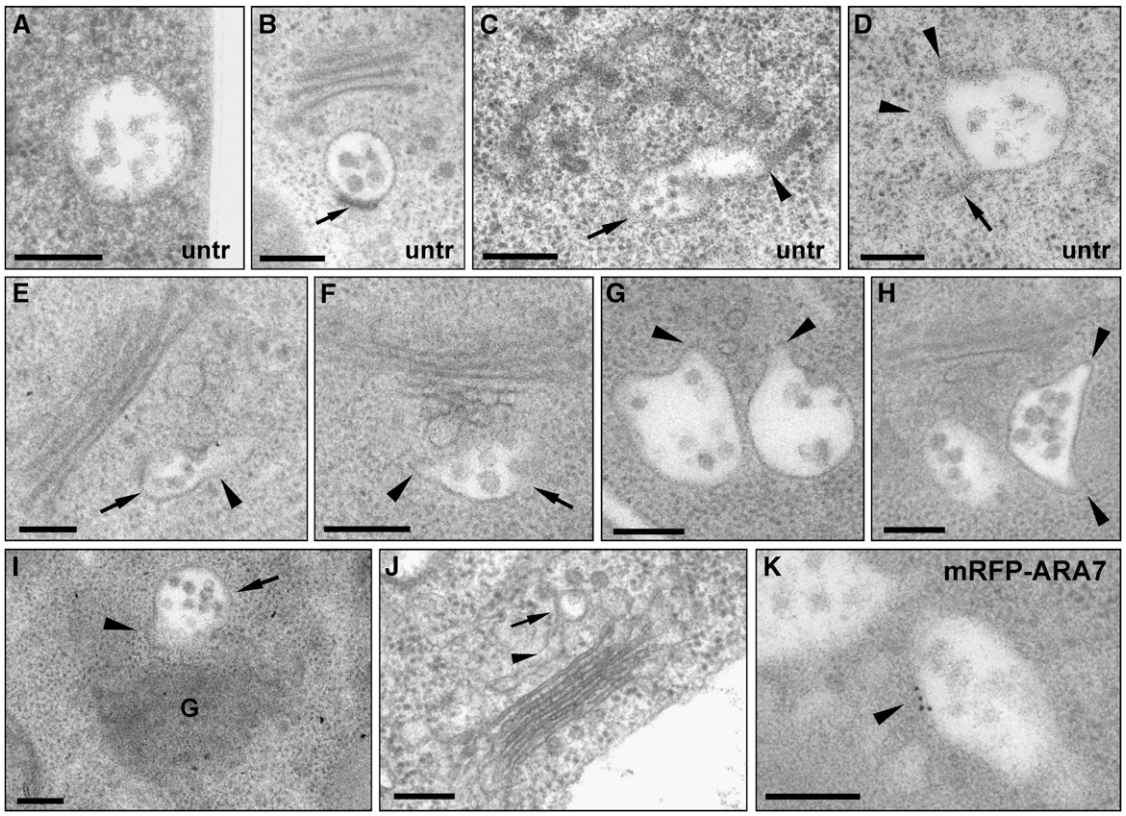

Figure 4. MVBs Mature from Tubular-Vesicular Structures.

(A) and **(B)** Mature MVBs in sections from high-pressure frozen untreated (untr) root cells typically have an almost perfect circular profile. Depending upon the plane of section, a plaque (arrow in **[B]**) is occasionally visible.
(C) An MVB (arrow) attached to a tubular-vesicular structure (arrowhead) in untreated *Arabidopsis* root tip cells.
(D) An MVB showing a tubular connection (arrow) and bottleneck terminations (arrowheads) in untreated *Arabidopsis* root tip cells.
(E) to **(H)** MVBs seen in *Arabidopsis* root tip cells during recovery from ConcA treatment (45 min ConcA; followed by 15-min washout) are pleiomorphic, often with bottleneck terminations. In **(E)** and **(F)**, MVBs (arrows) are attached to tubular structures (arrowheads) in the area of the TGN; in **(G)** and **(H)**, pleiomorphic MVBs display bottleneck terminations (arrowheads), indicating a possible connection to tubular structures above or beneath the plane of section.
(I) and **(J)** MVBs (arrows) directly connected to TGN-like structures (arrowheads). In **(J)**, root-tip cells were chemically fixed.
(K) mRFP-ARA7 localization at the limiting membrane of these unusually shaped (compared with **[A]** and **[B]**) multivesiculated structures confirms their identity as MVBs.
G, Golgi. Bars = 200 nm.

markers for the TGN/EE and the MVB/LE. During transient expression in protoplasts, fluorescent signals of both markers first became detectable 6 h after transfection. At this early time point, both markers mainly colocalized but their signals separated steadily over time (see Supplemental Figures 4A to 4C online), until they reached their typical distribution (Figure 8A; see Supplemental Figures 5A and 5B online).

To observe the spatio-temporal effect of VPS2-DN on the distribution of the MVB/LE marker mRFP-VSR2 and the TGN/EE marker YFP-SYP61, we analyzed different time points after transfection. After 14 h coexpression, VPS2-DN caused enlargement of the YFP-SYP61 signals, but TGN/EE and MVB/LE markers were still found to be separate (Figure 8B). However, 18 h after transfection, mRFP-VSR2 was mainly found to localize to the enlarged structures of the TGN (Figures 8C and 8D; see Supplemental Figures 5C and 5D online). Comparable effects were observed when VPS2-DN was coexpressed with YFP-SYP61 and the MVB/LE markers mRFP-ARA7 (Figures 8E to 8H; see Supplemental Figures 5E to 5H online) or ARA6-mRFP (Figures 8I to 8L; see Supplemental Figures 5I to 5L online). The effect of VPS2-DN expression on YFP-SYP61 and ARA6-mRFP distribution resulted in the highest observed r_p and r_s values, leaving almost no signals uncorrelated (Figure 8L; see Supplemental Figure 5L online; for comparison of all values, see Supplemental Figure 5M online). This temporal progression shows that VPS2-DN affects the TGN/EE first and suggests that the accumulation of the MVB/LE markers in the enlarged TGN/EE is due to perturbed MVB/LE maturation.

To demonstrate that the observed effects are specific for an inhibition of MVB maturation, we used an RNA interference

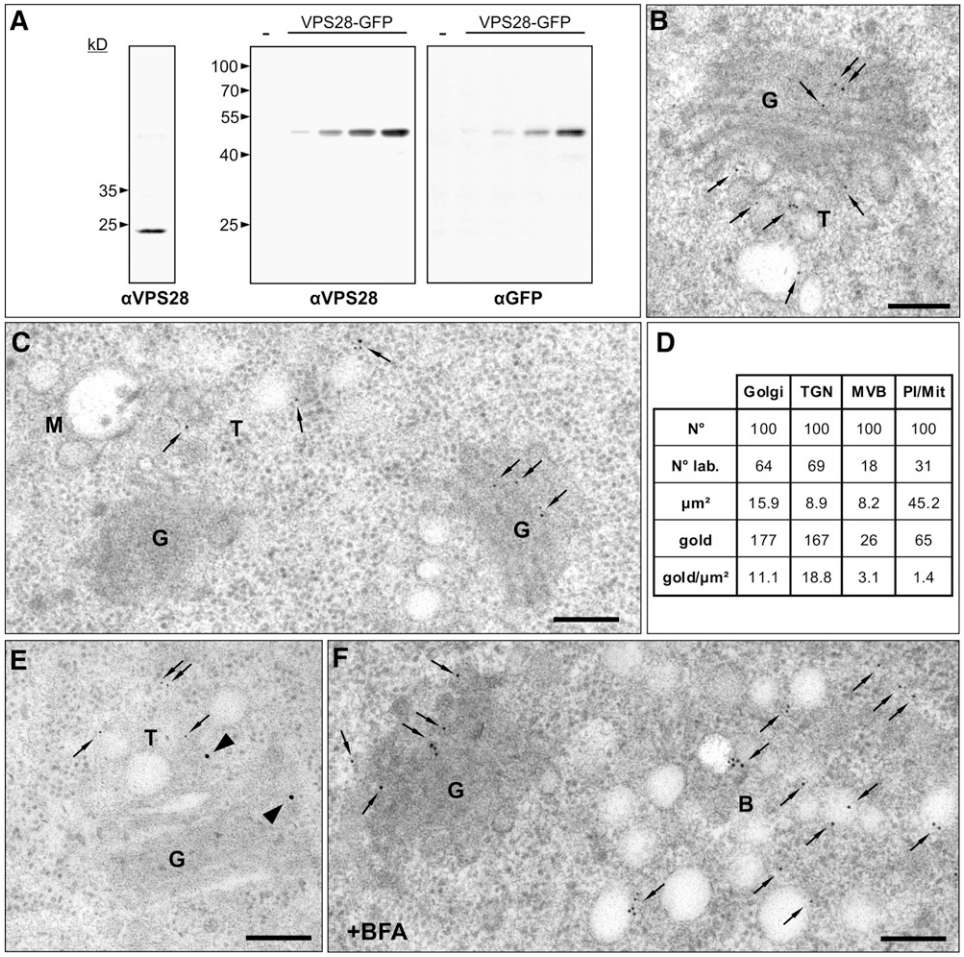

	Golgi	TGN	MVB	PI/Mit
N°	100	100	100	100
N° lab.	64	69	18	31
µm²	15.9	8.9	8.2	45.2
gold	177	167	26	65
gold/µm²	11.1	18.8	3.1	1.4

Figure 5. The ESCRT-I Component VPS28 Localizes to the Golgi and the TGN.

(A) Immunodetection of VPS28 in total protein extracts from 7-d-old *Arabidopsis* plants (left) using antibodies against VPS28 (αVPS28) and VPS28-GFP transiently expressed in protoplasts isolated from *Arabidopsis* suspension cultures (middle and right). Protoplasts were transfected with 3, 10, 30, or 100 μg plasmid DNA encoding for VPS28-GFP or mock transfected (−). Total protein extracts from protoplasts were probed with antibodies against VPS28 (αVPS28) and antibodies against GFP (αGFP).

(B) IEM analysis using the αVPS28 antibodies on high-pressure frozen *Arabidopsis* wild-type root cells shows that the endogenous VPS28 localizes to the Golgi stacks and the TGN (arrows).

(C) IEM of the endogenous VPS28 shows that VPS28 localizes to the Golgi stack and the TGN (arrows) but is not detected on the MVB

(D) Quantitative analysis of VPS28 IEM. The labeling density, expressed as the number of gold particles per micrometer^2 (gold/μm^2), is significantly higher for the TGN and the Golgi apparatus (18.8 and 11.1 gold/μm^2, respectively) compared to the MVBs (3.1 gold/μm^2) or plastids/mitocondria (1.4 gold/μm^2). N°, number of compartments encountered; N° lab., number of compartments labeled; μm^2, total area considered; gold, total number of gold particles detected; gold/μm^2, labeling density.

(E) Double immunolocalization of VPS28 in an *Arabidopsis* line expressing the TGN marker SYP61-CFP under the control of the endogenous promoter, using the polyclonal αVPS28 antibodies from rabbit in combination with 15-nm (arrowheads) gold-coupled secondary antibodies and monoclonal αGFP antibodies from mouse in combination with 5-nm (arrows) gold-coupled secondary antibodies. Both, the TGN marker and VPS28 localize to the same tubular-vesicular structure, immediately adjacent to the Golgi stacks.

(F) In BFA-treated *Arabidopsis* plants, VPS28 labels the core of the BFA compartment, confirming TGN localization of this ESCRT-I subunit.

G, Golgi; T, TGN; M, MVB/LE; B, BFA compartment. Bars = 200 nm.

(RNAi)-based knockdown of the retromer component sorting nexin 2a (RNAi-SNX2a). It was recently shown that RNAi-based SNX knockdown results in a change of VSR2 localization but does not affect vacuolar transport (Niemes et al., 2010a). In accordance with this, we could detect changes in the distribution of YFP-SYP61 and mRFP-VSR2, resulting in a fourfold increase of the r_p and r_s values (see Supplemental Figures 6A to 6D online). Moreover, no VPS2-DN–like effect was observed when RNAi-SNX2a was coexpressed with other markers for the MVB/LE. The distribution of YFP-SYP61 and mRFP-ARA7 (see Supplemental Figures 6E to 6H online) as well as YFP-SYP61 and ARA6-mRFP (see Supplemental Figures 6I to 6L online) remains unaltered when

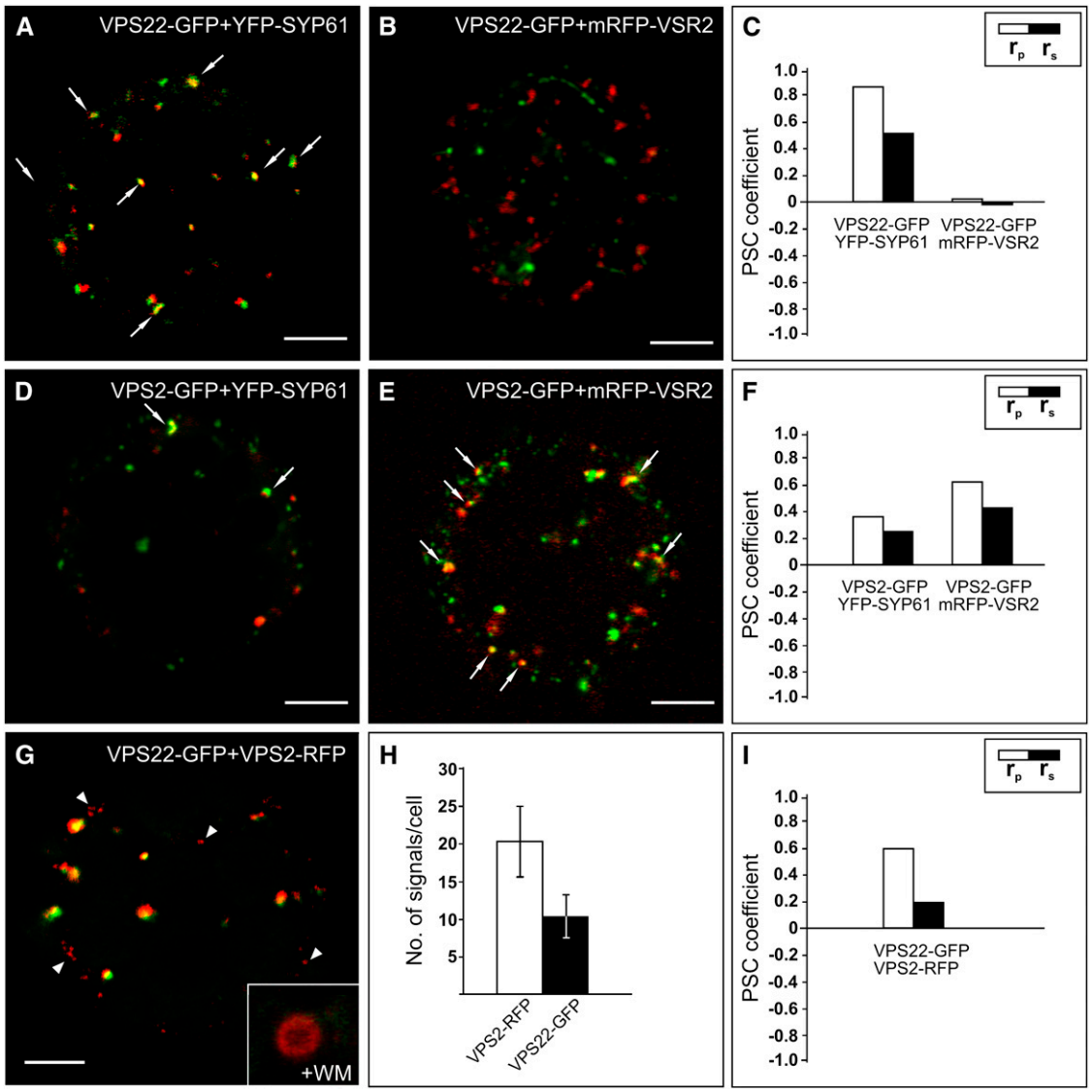

Figure 6. Gradual Distribution of the ESCRT-II Component VPS22 and the ESCRT-III Component VPS2.

Tobacco mesophyll protoplasts were transfected with plasmids encoding fluorescent markers/reporters as indicated below. Proteins were expressed for 18 to 24 h prior to CLSM analysis. White arrows indicate colocalization. For quantification, the PSC coefficients (r_p and r_s) were calculated after analysis of at least 10 individual protoplasts and a minimum of 200 signals. The level of colocalization ranges from +1 for perfect correlation to −1 for negative correlation. For the corresponding scatterplots of the fluorescence values of pixels across the two channels, see Supplemental Figure 2 online.

(A) Coexpression of VPS22-GFP and the TGN/EE marker YFP-SYP61.

(B) VPS22-GFP was coexpressed with the MVB/LE marker mRFP-VSR2.

(C) Quantification of VPS22-GFP colocalization with TGN/EE (YFP-SYP61) and MVB/LE (mRFP-VSR2) marker.

(D) Coexpression of VPS2-GFP and YFP-SYP61.

(E) VPS2-GFP and mRFP-VSR2 were coexpressed.

(F) Quantification of VPS2-GFP colocalization with TGN/EE and MVB/LE marker.

(G) Coexpression of VPS22-GFP and VPS2-RFP. Some VPS2-RFP signals do not colocalize (white arrowheads). Only VPS2-RFP signals localize to WM-sensitive compartments, as indicated by the magnified ring-like structure.

(H) Quantitative comparison of the number of VPS2-RFP and VPS22-GFP signals. Error bars indicate the SD of numbers of signals.

(I) Quantification of VPS22-GFP and VPS2-RFP colocalization.

Bars = 5 μm.

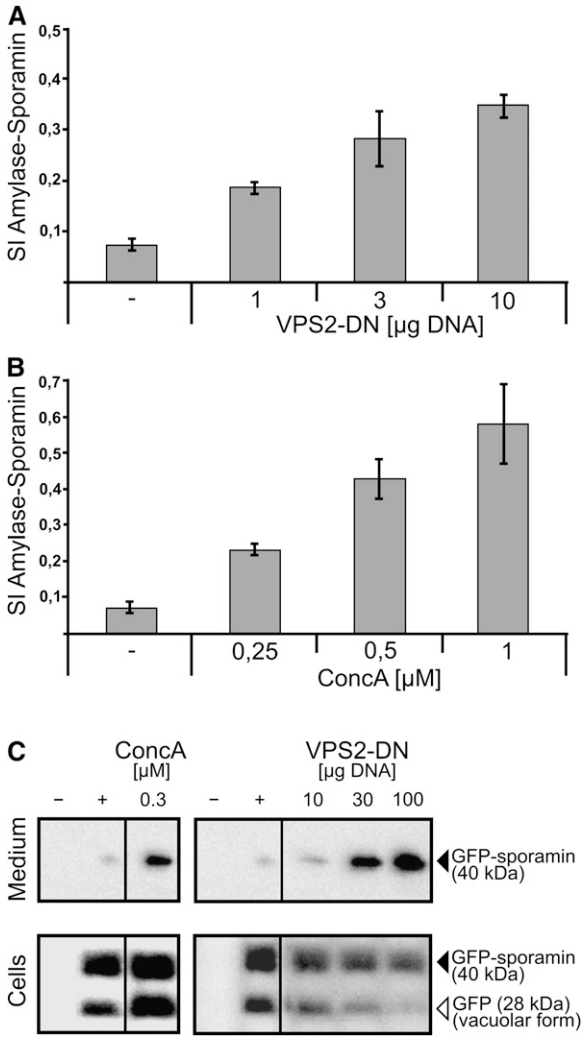

Figure 7. Effects of ConcA and the ESCRT-III Mutant VPS2-DN on Vacuolar Transport.

Tobacco mesophyll protoplasts were transfected with plasmids encoding for reporters/effectors, as indicated below. Proteins were expressed for 18 to 24 h prior to analysis. For analyzing vacuolar transport, the α-amylase derivative amylase-sporamin (amy-spo) was used. The SI is calculated as the ratio of the activity of amy-spo secreted to the culture medium and the activity of amy-spo within the cells.

(A) VPS2-DN causes a dosage-dependent mis-sorting of the vacuolar reporter amy-spo and subsequent secretion into the culture medium. Error bars indicate SD of five individual experiments.

(B) Treatment with increasing concentrations of ConcA leads to the same effect than described in **(A)** but stronger (10-fold increase of the SI). Error bars indicate SD of five individual experiments.

(C) Immunoblot analysis of protein transport after transient expression of the soluble vacuolar reporter GFP-sporamin in the presence of ConcA (left panel) or coexpression with VPS2-DN (right panel) using GFP-antibodies for immunodetection of the reporter. –, Mock transfection; +, positive control of GFP-sporamin expression without effector.

coexpressed with RNAi-SNX2a (for comparison, the values for all PSC coefficients are shown in Supplemental Figure 6M online).

ConcA Treatment and RNAi-Mediated Knockdown of the Annexin ANNAT3 Both Cause Increased Colocalization of TGN/EE and MVB/LE Markers

In mammals, it has been shown that Annexin A2, a calcium-dependent phospholipid binding protein, is involved in the last step of endosomal maturation in which the MVB is pinched off and released from the EE (Mayran et al., 2003). Therefore, we investigated if members of the plant annexin family might serve a similar function. The *Arabidopsis* genome encodes eight annexins (ANNAT1-8), and based on phylogenetic analysis, ANNAT3, 4, 5, and 8 are more closely related to human annexins. However, ANNAT5 and 8 are only expressed during pollen and embryo development and were thus excluded from further analysis (see Supplemental Figures 7A and 7B online). The potential function of ANNAT3 in MVB maturation was analyzed by RNAi in protoplasts expressing YFP-SYP61 as TGN/EE and mRFP-VSR2 as MVB/LE markers. Coexpression of both markers with RNAi-ANNAT3 increases the values of the PSC coefficients from $r_p = 0.14$ and $r_s = -0.09$ to $r_p = 0.51$ and $r_s = 0.28$ (cf. Figures 9A to 9C with 9G to 9I), as a result of the reduced transcript level of the endogenous annexin (see Supplemental Figure 7C online). ConcA treatment also results in increased values of the PSC coefficients (Figures 9D to 9F), which is in agreement with the observed effect of ConcA on the TGN/MVB marker distribution in stably transformed plants (see Supplemental Figure 1 online).

DISCUSSION

V-ATPase Activity and TGN Integrity Are Required for Vacuolar Transport and MVB Formation

Binding of the VSR BP80 to an affinity column using the vacuolar sorting motif NPIR from barley (*Hordeum vulgare*) proaleurain as bait occurred at neutral pH and was abolished at acidic pH (Kirsch et al., 1994). Based on this finding and the progressive acidification in the secretory and endocytic pathway of mammalian cells (Mellman et al., 1986), it has been postulated that binding of vacuolar cargo to VSRs takes place in the TGN, whereas dissociation would take place in the more acidic MVBs (Paris et al., 1997). However, it is important to note that, at least to our knowledge, pH has neither been measured directly for the TGN/EE nor the MVB/LE of plant cells. The finding that a high density of V-ATPase complexes is found at the TGN/EE rather than at the MVB/LE (Dettmer et al., 2006) suggests that the TGN is an acidic compartment making it unfavorable for the binding of vacuolar cargo to VSRs. A more appropriate upstream location for receptor–ligand interaction could be the endoplasmic reticulum, since vacuolar cargo is retained in the endoplasmic reticulum when the luminal domain of VSRs is anchored to an endoplasmic reticulum membrane protein (Niemes et al., 2010a). On the other hand, the relative lack of V-ATPase complexes in MVB/LEs (Dettmer et al.,

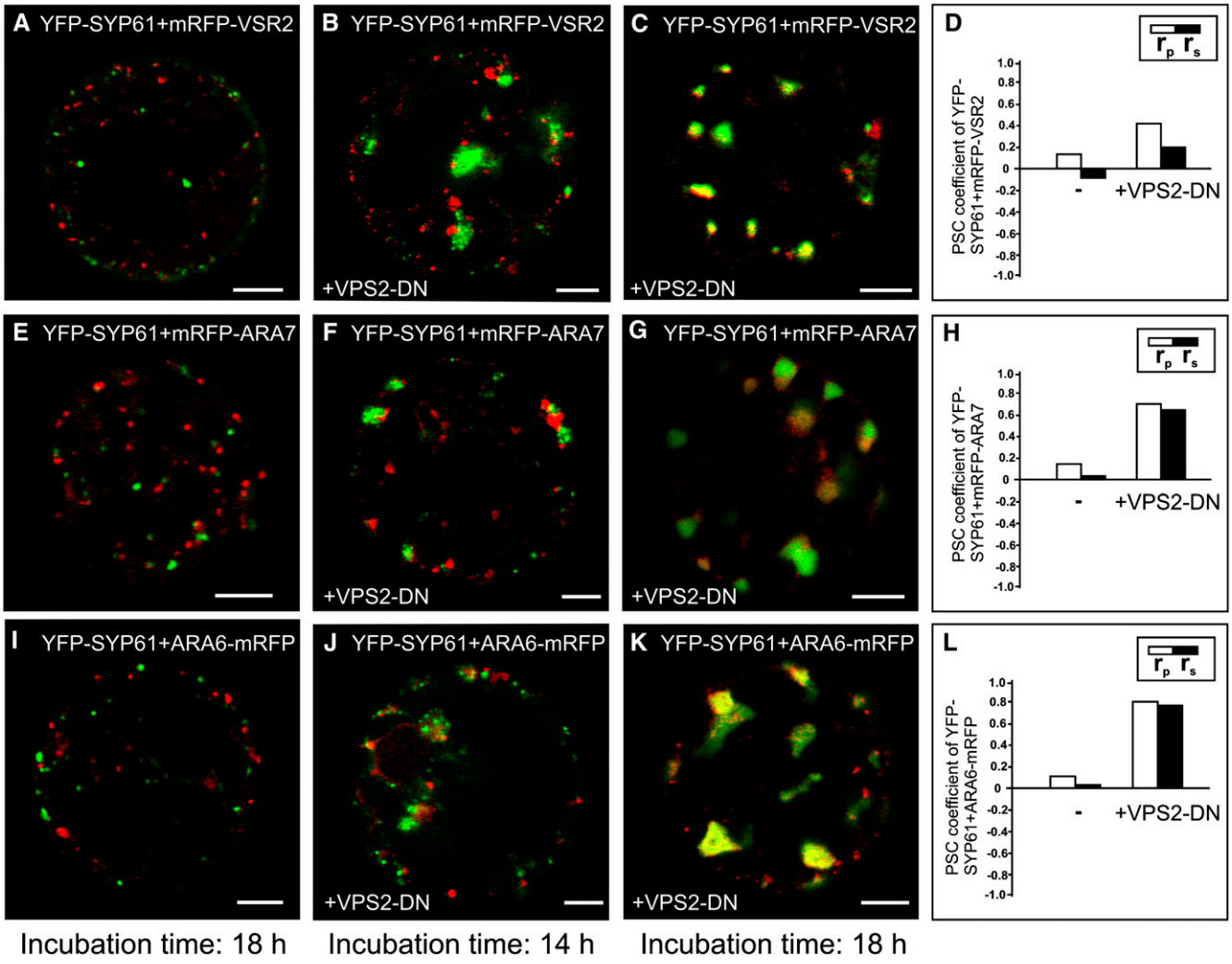

Figure 8. VPS2-DN Causes Marker Proteins for TGN/EE and MVB/LE to Colocalize.

Tobacco mesophyll protoplasts were transfected with plasmids encoding for fluorescent markers/reporters as indicated below. Proteins were expressed for 18 h prior to CLSM analysis. For quantification, the PSC coefficients (r_p and r_s) were calculated after analysis of at least 10 individual protoplasts and a minimum of 200 signals. The level of colocalization ranges from +1 for perfect correlation to −1 for negative correlation. For the corresponding scatterplots of the fluorescence values of pixels across the two channels, see Supplemental Figure 5 online.

(A) Coexpression of TGN/EE and MVB/LE markers YFP-SYP61 and mRFP-VSR2 18 h after transfection.

(B) Effect of VPS2-DN on the distribution of TGN/EE and MVB/LE markers 14 h after transfection.

(C) Analysis 18 h after transfection: VPS2-DN causes a change in the signal pattern of the marker proteins. The signals accumulate in bigger but fewer structures.

(D) Quantification of the marker colocalization. The r_p and r_s values increase when VPS2-DN is expressed.

(E) Coexpression of TGN/EE and MVB/LE markers YFP-SYP61 and mRFP-ARA7 18 h after transfection.

(F) Effect of the VPS2-DN coexpression with YFP-SYP61 and mRFP-ARA7 14 h after transfection.

(G) When expressed for 18 h, VPS2-DN increases colocalization of YFP-SYP61 and mRFP-ARA7. As observed in **(C)**, the signals change structurally.

(H) Quantification reveals higher r_p and r_s values for the marker proteins when VPS2-DN is expressed.

(I) to **(L)** An experiment as described in **(E)** to **(H)** was performed, except ARA6-mRFP was used as MVB/LE marker. Here, the highest increase of r_p and r_s values is found **(L)**.

Bars = 5 μm.

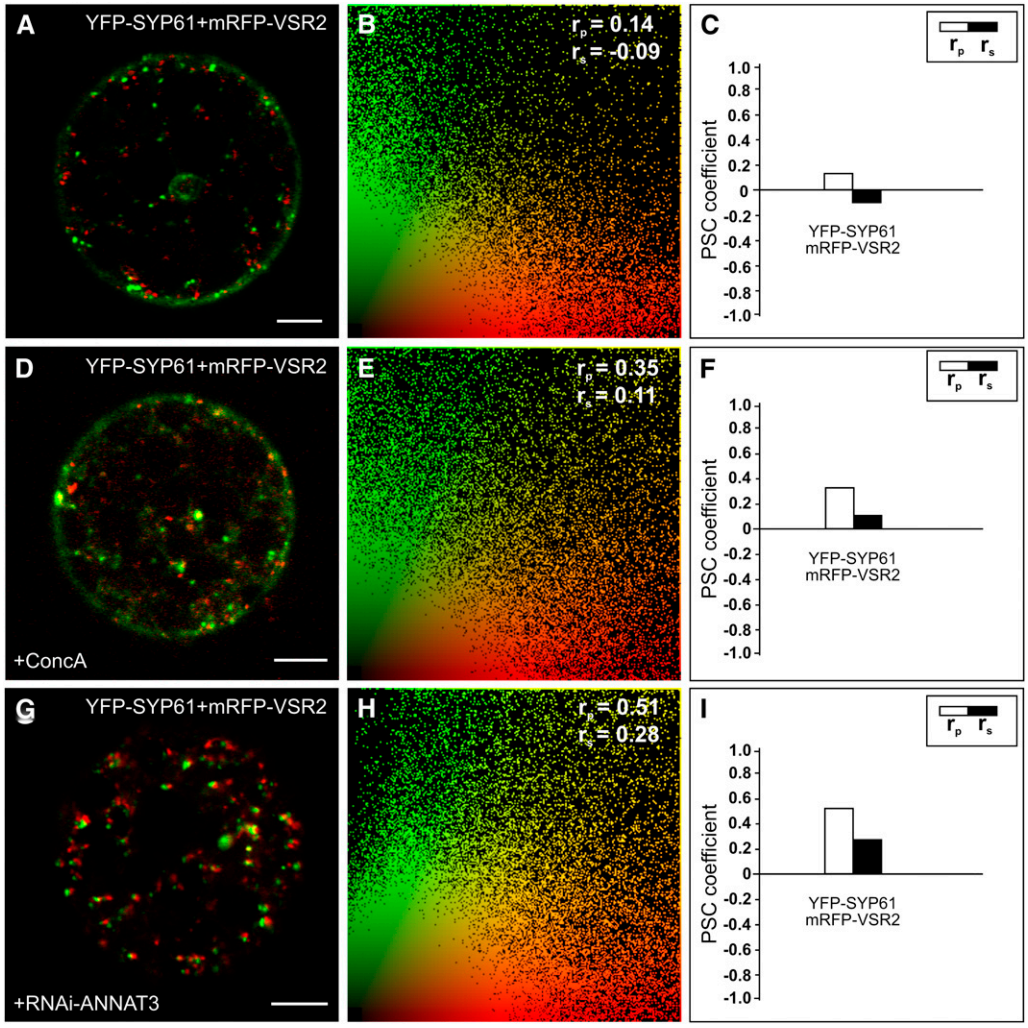

Figure 9. RNAi Knockdown of the Annexin ANNAT3 Increases Colocalization of TGN/EE and MVB/LE Marker Proteins.

Tobacco mesophyll protoplasts were transfected with plasmids encoding for fluorescent markers/reporters as indicated below. Proteins were expressed for 18 to 24 h prior to CLSM analysis. For quantification, the PSC coefficients (r_p and r_s) were calculated after analysis of at least 10 individual protoplasts and a minimum of 200 signals. The level of colocalization ranges from +1 for positive correlation to −1 for negative correlation, and the fluorescence values of pixels across the two channels are depicted in an intensity scatterplot.

(A) Tobacco protoplast expressing YFP-SYP61 as TGN/EE marker and mRFP-VSR2 as MVB/LE marker.

(B) Intensities of fluorescent signals from **(A)**, representing YFP-SYP61 (green) and mRFP-VSR2 (red), are depicted in a scatterplot. The calculated PSC values are given in the top right corner.

(C) Bar chart to illustrate the PSC coefficients from **(B)**.

(D) Protoplasts from **(A)** were incubated for 1 h in the presence of 1 μM ConcA.

(E) Intensities of fluorescent signals from **(D)**, representing YFP-SYP61 (green) and mRFP-VSR2 (red), are depicted in a scatterplot. The calculated PSC values are given in the top right corner.

(F) Bar chart to illustrate the PSC coefficients from **(E)**.

(G) RNAi-based knockdown of ANNAT3 by cotransfection of plasmid DNA encoding for RNAi-ANNAT3 and the markers YFP-SYP61 and mRFP-VSR2.

(H) Intensities of fluorescent signals from **(G)**, representing YFP-SYP61 (green) and mRFP-VSR2 (red), are depicted in a scatterplot. The calculated PSC values are given in the top right corner. The r_p and r_s values are considerably higher compared with the control **(B)**.

(I) Bar chart to illustrate the PSC coefficients from **(H)**.

Bars = 5 μm.

2006) does not necessarily mean that the pH in MVBs is any less acidic than in the TGN. If, as we postulate, MVBs/LEs are released from the TGN/EE, their pH would not change during this process, since it was established already in the TGN/EE.

Although a role for the V-PPase or a P-type H^+-ATPase in the MVBs can at the present not be excluded, several lines of evidence indicate that V-ATPase–dependent acidification is required for the structure and function of the TGN/EE. ConcA inhibits the V-ATPase and blocks vacuolar transport (Matsuoka et al., 1997; Dettmer et al., 2006). This treatment prevents the formation of the TGN/EE and causes the retention of TGN/EE proteins in an enlarged Golgi stack (Dettmer et al., 2006; Viotti et al., 2010). By contrast, V-ATPase proteins are not detectable in MVBs by immunostaining either in CLSM or EM analysis, and the structure of MVBs remains unchanged after ConcA treatment. However, the number of MVBs was found to be drastically reduced after short-term inhibition of the V-ATPase. The decreased number suggests that MVBs/LEs are nonpersistent transport carriers that are continuously formed at the TGN/EE and as the ultrastructural analysis shows, are ultimately consumed through fusion with the vacuole. It also means that V-ATPase activity at the TGN/EE is required for MVB/LE biogenesis.

As suggested by our ultrastructural analysis of TGN regeneration after ConcA washout, MVB formation and separation from the TGN appears to be a rapid event and, therefore, difficult to capture under normal conditions. However, budding of MVBs from tubular, putative TGN structures is not restricted to recovery from drug treatment situations but can also be seen under physiological conditions. This is in agreement with earlier observations, that dilations of the partially coated reticulum (Pesacreta and Lucas, 1984; Hillmer et al., 1988) contain intralumenal vesicles (Tanchak et al., 1988). A recent electron tomographic analysis of the TGN (Kang et al., 2011) failed to provide evidence for the formation of MVBs, although it was speculated that the membrane fragments that arise as a result of TGN fragmentation may become precursors of MVBs. According to Kang et al. (2011), the TGN dissociates from the stack and disintegrates into three parts: smooth vesicles (SVs), CCVs, and tubules, which connected both putative carriers prior to fragmentation. The SVs are considered to carry secretory cargo but also recycle receptors to the PM; by contrast, the CCV would transport endocytosed PM receptors destined for degradation first to MVBs and then to the vacuole. However, there are several problems with this model. First, it excludes entirely a role for the TGN in the transport of anterograde cargo proteins to the vacuole. Second, it goes against the well-established fact that in mammalian cells, PM receptors are recycled from the EE by CCVs and not SVs (Stoorvogel et al., 1996; van Dam and Stoorvogel, 2002). Third, it does not take into account the dynamics of the relationship between the TGN and the Golgi as previously observed by Viotti et al. (2010) in a live-cell imaging analysis.

MVB/LE Maturation: An Alternative Model for Transport toward the Lytic Vacuole

According to current concepts, lytic enzymes are recognized by VSRs at the TGN and become packaged into CCVs for anterograde transport to the MVB (Foresti et al., 2010; Kim et al., 2010; Saint-Jean et al., 2010; Zouhar et al., 2010). This model is based on analogy to mammalian cells, in which lysosomal acid hydrolases are recognized in the TGN by mannosyl 6-phosphate receptors and then sequestered into CCVs and transported to the EE (Braulke and Bonifacino, 2009). After ligand dissociation, the mannosyl 6-phosphate receptors are returned to the TGN with the help of SNXs and retromer (Bonifacino and Hurley, 2008; Mari et al., 2008). However, the EE of mammalian cells characteristically has extensive tubular protrusions, many of which end in CCVs in which internalized PM receptors collect to be recycled to the PM (van Meel and Klumperman, 2008). Thus, in mammalian cells, CCVs are formed at both the TGN and the EE with different functions at each compartment. Does the TGN/EE hybrid in plants have two different classes of CCVs? A final decision on this cannot be taken at present: Not only do we lack evidence for CCV-mediated transport to the PM from so-called recycling endosomes, but even more importantly in this context, there is no unequivocal proof that TGN-derived CCVs in plants carry VSRs. Indeed, the recent reports of VSRs at the PM (Saint-Jean et al., 2010; Wang et al., 2011) suggest that the VSRs originally isolated from fractions enriched in CCVs (Kirsch et al., 1994) may actually have been present in endocytic CCVs. Our experiments with clathrin hub expression strengthen the notion that anterograde traffic to the vacuole does not require the participation of CCVs and, as a consequence, occurs without the recycling of receptors from a post-TGN compartment as recently proposed by Niemes et al. (2010a).

A widely accepted feature of the mammalian endocytic pathway is that transport of lysosomal acid hydrolases after entry into the EE is receptor independent and occurs by gradual maturation of the EE into the LE followed by fusion with the lysosome (Piper and Katzmann, 2007; van Weering et al., 2010). The notion that a similar maturation-based sorting process may take place in the plant endocytic pathway has only recently been considered by plant scientists (Niemes et al., 2010b), and the data presented here indicate that the mechanism and the molecular machinery involved in endosomal maturation might be conserved between animals and plants.

Molecules Involved in MVB Maturation: Rabs, ESCRT, and Annexins

In mammalian cells, maturation of LEs from EEs is triggered by a Rab conversion mechanism in which the EE-localized Rab5 is replaced by SAND-1/Mon1, which in turn recruits Rab7, resulting in a Rab7-positive LE (Rink et al., 2005; Poteryaev et al., 2010). Whether a comparable mechanism also functions in plants is a matter for speculation. Plant MVBs/LEs possess the Rab5-type GTPases ARA6/7 (Haas et al., 2007), while Rab11-type class A/B Rabs are found at the TGN/EE (Chow et al., 2008). However, a protein with similarity to the Rab exchange protein SAND-1/Mon1 is encoded in the *Arabidopsis* genome, and its functional analysis will hopefully reveal if a similar mechanism is indeed operational in plants. Nevertheless, when MVB maturation is blocked, an MVB/LE marker should become detectable at the TGN/EE, and this does indeed occur. We have shown that the ConcA-induced inhibition of protein transport at the TGN (Dettmer et al., 2006; Viotti et al., 2010) markedly shifts the steady state

distribution of the predominantly MVB/LE-localized proteins mRFP-ARA7 and ARA6-mRFP toward the TGN/EE.

The characteristic internal vesicles of MVBs originate as a result of ESCRT-mediated vesicle budding from the limiting membrane into the lumen of endosomes (Hurley and Hanson, 2010). In this process, ESCRT-0 clusters cargo, ESCRT-I and -II induce the formation of buds and sequester cargo into them, and ESCRT-III finally mediates vesicle fission (Hurley and Hanson, 2010; Wollert and Hurley, 2010). Our EM data, showing the formation of MVBs/LEs at the TGN/EE, suggest that the ESCRT machinery might already act at this early developmental stage. To test for this, we have ultrastructurally analyzed the localization of VPS28 in high-pressure frozen *Arabidopsis* root cells. This ESCRT-I component localizes to the Golgi and the TGN/EE but not to the MVB/LE, demonstrating that ESCRT-mediated sorting and, thus, the formation of ILVs is not restricted to the MVB/LE.

We have furthermore analyzed tobacco protoplasts transiently coexpressing the fluorescently tagged ESCRT-II or -III subunits VPS22-GFP or VPS2-GFP with fluorescent markers for the TGN/EE and MVB/LE. The majority of fluorescent signals of VPS22-GFP colocalized with the TGN/EE marker, while colocalization with the MVB/LE marker was low. By contrast, VPS2-GFP signals were found to colocalize mainly with the MVB/LE marker but occasionally also with the TGN marker. However, almost all ESCRT-II VPS22 signals colocalized with ESCRT-III VPS2 signals, supporting the participation of ESCRT in the early development of MVBs/LEs. The reason for this differential distribution of ESCRT subunits could be explained by different requirements for their release from membranes. This has indeed been shown for yeast ESCRTs, where the disassembly of ESCRT-III, but not of earlier ESCRTs, is strictly dependent on the AAA-ATPase Vps4 (Nickerson et al., 2010). SKD1, the *Arabidopsis* homolog of Vps4, localizes to MVBs/LEs (Haas et al., 2007) and interacts with ESCRT-III and ESCRT-associated proteins, but not with ESCRT-I or -II subunits (Spitzer et al., 2009; Shahriari et al., 2010). Therefore, the localization of the ESCRT-III subunit VPS2 at the MVB/LE is in agreement with the localization of the ESCRT-associated AAA-ATPase.

To understand better the role of the ESCRT machinery for the transport of vacuolar cargo between the TGN/EE and the MVB/LE, we generated a VPS2 mutant (VPS2-DN). Expression of this mutant in tobacco protoplasts blocks transport of the soluble vacuolar reporter molecules amy-spo or GFP-spo in a dose-dependent manner. This effect is comparable to that of an ATP hydrolysis-deficient mutant of SKD1 (Shahriari et al., 2010). Coexpression of the mutant with the TGN/EE marker YFP-SYP61 and the MVB/LE cargo mRFP-VSR2 yielded their colocalization in large structures, indicating that protein transport from the TGN/EE to the MVB/LE is blocked. Interestingly, the loss of Class E vps (vacuolar protein sorting) genes (Raymond et al., 1992), all of which encode for ESCRT and ESCRT-associated proteins (Katzmann et al., 2001; Babst et al., 2002a, 2002b; Bilodeau et al., 2002), results in the formation of exaggerated prevacuolar organelles, termed class E compartments (Raymond et al., 1992). In mammalian cells, these compartments are of early endosomal origin, accumulate EE markers, endocytosed receptors, and lysosomal proteins (Yoshimori et al., 2000; Doyotte et al., 2005) and have therefore been referred to as multicisternal EEs (Doyotte et al., 2005).

VSR-based MVB/LE cargo molecules accumulate at the TGN/EE, when retromer-mediated recycling is perturbed after RNAi knockdown of the sorting nexin SNX2a (Niemes et al., 2010b). However, in this situation, vacuolar transport via the MVB/LE is not blocked. Therefore, we considered it necessary to determine whether the VPS2-DN–induced transport inhibition between TGN and MVB/LE was indeed due to a block in the transport route, rather than to an interaction between mRFP-VSR2 and the ESCRT machinery. Coexpression of VPS2-DN with the MVB/LE markers ARA6-mRFP or mRFP-ARA7, which are recruited from the cytosol onto their target membranes, also resulted in their colocalization with the TGN/EE marker in enlarged structures, suggesting inhibited maturation of the MVB/LE. Similar effects were seen during RNAi-induced knockdown of the annexin ANNAT3. In mammalian cells, annexin A2 has been shown to be required for the fission of MVBs from the EE in a process downstream of the ESCRT-mediated budding of intralumenal vesicles (Mayran et al., 2003). This process requires the Annexin A2–dependent polymerization of actin (Morel and Gruenberg, 2009). On the basis of our EM data, showing MVBs/LEs containing bottleneck structures after ConcA washout, it is tempting to speculate that such structures might be a target for annexin action. However, the function of plant annexins with respect to the modulation of membrane dynamics remains to be established (Laohavisit and Davies, 2011).

In the past, post-Golgi protein trafficking to the vacuole in plants has been considered to occur through vesicles moving between stable compartments: the TGN/EE and the MVB/LE. Although a fusion of the MVB/LE with the vacuole has been previously discussed, the consequence of this event (i.e., the replenishment

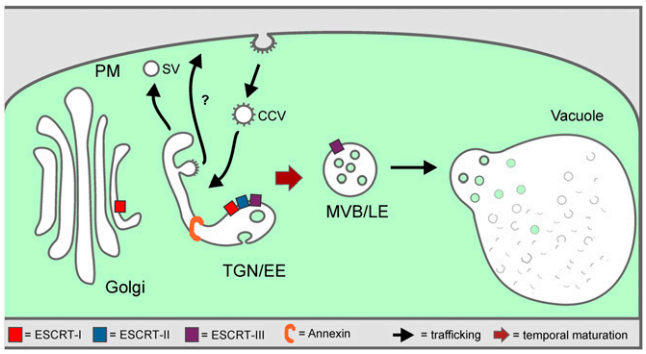

Figure 10. Model Illustrating MVB Maturation from the TGN.

According to this model, the TGN is continually formed and released from the Golgi stack. It also functions as an EE and receives incoming cargo from the PM via CCVs. As it differentiates, the TGN probably subdivides into domains where SVs are released to the PM, into domains releasing CCVs for recycling to the PM (recycling endosomes) and into a domain that matures into an MVB. Participating in the latter process, as indicated, are the ESCRT complexes I, II, and III, as well as annexin. As in mammalian cells, we postulate that post-TGN trafficking of soluble proteins to the lytic compartment (vacuole) occurs receptor independently and is accompanied by a gradual transformation of parts of the EE (TGN) into the LE (MVB), which ultimately fuses with the vacuole membrane.

of the MVB/LE population) has not been addressed. Here, we provided evidence pointing to a continual nonvesicular flux of membrane from the TGN to the MVB. Thus, when the structure and integrity of the TGN is perturbed, MVB formation is inhibited. As in mammals, the endosomal system of plants is not a static set of clearly separable structures but characterized by the dynamic generation and consumption of membrane compartments that are derived from each other by maturation (Figure 10).

METHODS

Plant Materials and Growth Conditions

Tobacco plants (*Nicotiana tabacum* var SR1) were grown as previously described (Pimpl et al., 2006). Suspension cultures of *Arabidopsis thaliana* var Landsberg *erecta* PSB-D and tobacco Bright Yellow 2 stably expressing GONST1-YFP or GFP-BP80 (Tse et al., 2004) were cultivated as described (Miao et al., 2006; Miao and Jiang, 2007) and used 3 d after subculturing. *Arabidopsis* ecotype Columbia-0 was used for IEM and CLSM analysis. *Arabidopsis* seedlings were grown on Murashige and Skoog (MS) medium supplemented with 1% Suc at 22°C, with cycles of 16 h light for 4 to 5 d. For ConcA treatments, seedlings were incubated in 1 mL of liquid medium (half-strength MS medium with 0.5% Suc, pH 5.8) containing 1 μM ConcA for 45 min, at room temperature. For the washout, seedlings were immerged in fresh liquid medium for 15 min. The ConcA stock solution was 1 mM in DMSO. WM was added 1 h prior to CLSM analysis in 30 μM concentration. The stock solution was 20 mM in DMSO.

Plasmid Constructs and Plant Transformation

Established plasmids were used encoding for markers/reporters as indicated: mRFP-VSR2 (Miao et al., 2008), YFP-SYP61 (Uemura et al., 2004), Man1-RFP (Nebenführ et al., 1999), GFP-sporamin (daSilva et al., 2005), mRFP-ARA7 and ARA6-mRFP (Ueda et al., 2004), and α-amylase-sporamin (Pimpl et al., 2003). For new recombinant plasmids, all DNA manipulations were performed according to established procedures. Coding sequences were amplified by PCR from either first-strand cDNA prepared from 3-d-old seedlings (Pimpl et al., 2003) or existing plasmid DNA. Recipient vectors were cut according to the restriction sites of the fragments and dephosphorylated prior to ligation. The *Escherichia coli* strain MC1061 (Casadaban and Cohen, 1980) was used for the amplification of all plasmids. The coding sequences of VPS2 and VPS22 were amplified from cDNA with *Nhe*I and *Not*I restriction sites using the VPS2-GFP.FOR and the VPS2-GFP.REV primers for *VPS2* and the VPS22-GFP.FOR and the VPS22-GFP.REV primers for *VPS22* and then ligated in the accordingly cut vector pSN9 (encoding for SNX2a-GFP; Niemes et al., 2010b) to produce GFP fusions. For an RFP fusion of VPS2, the coding sequence was amplified from VPS2-GFP with *Bgl*II and *Xba*I restriction sites using the VPS2-RFP.FOR and the VPS2-RFP.REV primers and then ligated in the plasmid pBP30 (Nebenführ et al., 1999) cut the same way. The truncated VPS2 (VPS2-DN) was constructed using the VPS2-DN.FOR and VPS2-DN.REV primers for amplification from VPS2-GFP, resulting in a 41-bp shorter coding region and then ligated with *Cla*I and *Xba*I restriction sites into pSar1 (Phillipson et al., 2001). To generate the RNAi construct of *ANNAT3*, the wild-type gene was amplified from *Arabidopsis* cDNA using the primers ANNAT3-WT.FOR and ANNAT3-WT.REV. The primers created an N-terminal *Nhe*I and a C-terminal *Sal*I restriction site for insertion into the pSN13 donor vector (Niemes et al., 2010b). The RNAi construct was then generated by cloning a C-terminal 178-bp fragment (from C754 to C932) of the *ANNEXIN* wild-type construct in sense and antisense orientations, linked by the PDK intron of pHannibal, into pGD5 (Niemes et al., 2010b). All constructs were verified by sequencing.

For the generation of a stably transformed *Arabidopsis* line expressing mRFP-ARA7, the coding sequence of ARA7 was amplified using primers mRFP-ARA7.FOR and mRFP-ARA7.REV. This fragment was then cloned into the *Bgl*II/*Bam*HI sites of pURTkan, a derivative of pJHA212 (Yoo et al., 2005), containing the Ubiquitin 10 promoter and the mRFP coding sequence. The resulting binary plasmid was introduced into *Agrobacterium tumefaciens* strain GV3101:pMP90 and selected on 5 mg/mL rifampicin, 10 mg/mL gentamycin, and 100 mg/mL spectinomycin. Columbia-0 plants were transformed according to Clough and Bent (1998), and transgenic plants were selected on MS medium with 1% Suc and 50 mg/mL kanamycin. All primers used for cloning are shown in Supplemental Table 1 online. The stably transformed *Arabidopsis* line expressing SYP61-CFP under the endogenous promoter (Robert et al., 2008) was kindly provided by Natasha Raikhel.

Generation of Antibodies

The coding sequence of *Arabidopsis* VPS28 and VPS2 was amplified from cDNA using the primer pairs VPS28.FOR/VPS28.REV and VPS2.FOR/VPS2.REV, respectively, and then ligated into the glutathione *S*-transferase (GST) expression vector pGEX-4T3 (accession U13855) previously cut with *Eco*RI/*Sal*I. The GST fusion proteins were expressed for 3 h in *E. coli* BL21 after induction with 1 mM isopropyl β-D-1-thiogalactopyranoside. Inclusion bodies containing GST-VPS28 or GST-VPS2 were solubilized using an established protocol with *N*-laurylsarcosine (Frangioni and Neel, 1993). The recombinant proteins were then affinity purified with GST-sepharose. For further purification, SDS-PAGE was performed, and the protein bands of interest were excised and electro-eluted from the gel using an Elutrap Electroelution System (Whatman) at 4°C with 50 mA for 16 h. Eluted proteins were dialyzed three times for 2 h against TBS (50 mM Tris and 152 mM NaCl, pH 7.4) prior to lyophilization. Three hundred milligrams of each lyophilized GST-fusion protein was used for commercial immunization of rabbits (Eurogentec). All primers used for cloning are shown in Supplemental Table 1 online.

Protein Extraction and Gel Blot Analysis

Seven-day-old *Arabidopsis* plants were frozen in liquid N_2 and homogenized with glass beads in a TissueLyser II (Qiagen) in extraction buffer containing 100 mM Tris, pH 7.8, 200 mM NaCl, 1 mM EDTA, 2% (v/v) β-mercaptoethanol, and 0.2% (v/v) Triton X-100. Protein gel blots and immunodetection were performed on total cell extracts processed as described previously (Pimpl et al., 2006). The polyclonal antiserum raised against VPS28 was used in a 1:10,000 dilution, and the VPS2 antiserum was diluted 1:2500. Monoclonal antibodies against GFP (Roche) were diluted 1:1000.

Isolation of Protoplasts and Transient Gene Expression

Tobacco mesophyll protoplasts were isolated from leaves of 6- to 8-week-old plants and subsequently transfected via electroporation as described previously (Bubeck et al., 2008). Unless otherwise stated, 10 μg of plasmid DNA were use for transfection, and protoplasts were incubated for 16 to 24 h. *Arabidopsis* protoplasts were generated from cell suspension cultures 3 d after subcultivation and subsequently transformed either via polyethylene glycol–mediated transformation as described before (Negrutiu et al., 1987) or via electroporation as previously described (Niemes et al., 2010a). Twenty micrograms of plasmid DNA were used for each transformation. Afterwards, the protoplasts were incubated in the dark at 26°C for a minimum of 20 h.

Fluorescence-Assisted Cell Sorting and RT-PCR

Tobacco protoplasts expressing cytosolic GFP alone or coexpressing the RNAi-ANNAT3 plasmid for 24 h were subjected to fluorescence-assisted cell sorting using a MoFlo flow cytometer (Beckman-Coulter). A total of 70,000 fluorescent protoplasts were sorted for each condition using a 100 μM nozzle. The sheath solution was PBS at pH 7.0, and the core/sheath was operated at 30.7 p.s.i./30.0 p.s.i., respectively. GFP fluorescence was excited with a standard 488-nm argon laser powered to 50 mW. Emission was detected in FL1 (504 to 522 nm) and plotted against FL2 (565 to 605 nm) to spread signals derived from GFP and autofluorescence. Autofluorescence signals were gated out by analyzing a mock-transfected protoplast population. Data acquisition and analysis were performed using the MOFLO Summit 4.3 software. For each condition, total RNA from 70,000 sorted protoplasts was extracted using the RNeasy plant mini kit (Qiagen) according to the instructions of the manufacturer, and 250 ng of the total RNA was used for the synthesis of first-strand cDNA (RevertAid H Minus first-strand cDNA synthesis kit; Fermentas). RT-PCR for ANNEXIN1 or ANNEXIN3 from tobacco was performed with the primer pairs NtAnx1.FOR/NtAnx1.REV or NtAnx3.FOR/NtAnx3.REV. Actin was amplified as a control using the primer pair Actin.FOR/Actin.REV.

Confocal Microscopy and Immunofluorescence Labeling

Imaging was performed using a Zeiss Axiovert LSM 510 Meta confocal laser scanning microscope and C-Apochromat ×63/1.2-W corrective water immersion objective. At the metadetector, main beam splitters (HFT) 405/514, 458/514, and 488/543 were used. The following fluorophores (excited and emitted by frame switching in the multitracking mode) were used: GFP, 488 nm/496 to 518 nm; YFP, 514 nm/529 to 550 nm; and RFP, 543 nm/593 to 636 nm. Pinholes were adjusted to 1 Airy unit for each wavelength. Postacquisition image processing was performed using the Zeiss LSM 510 image browser (4.2.0.121) and Corel-DrawX4 (14.0.0.567) (Corel).

For immunofluorescence analysis, Bright Yellow 2 cells were fixed and processed as previously described (Ritzenthaler et al., 2002). Samples were incubated overnight at 4°C with the VPS2 antibodies diluted at 1:200. The Alexa-Fluor 546 conjugate (Invitrogen) was used as secondary antibody.

Statistical Analysis of CLSM Localization Data

For statistical analysis, the PSC colocalization plug-in (French et al., 2008) for ImageJ (Abramoff et al., 2004) was used to calculate the linear Pearson correlation coefficient (r_p) and the nonlinear Spearman's rank correlation coefficient (r_s) of red and green fluorescent signals. Values were between −1 (negative correlation) and +1 (positive correlation). The fluorescence values of all pixels across the two channels of all analyzed signals were depicted in a scatterplot. Masking of areas of was performed with the ImageJ brush tool as described by French et al. (2008). For every analyzed image, punctuate signals were selected and the threshold level, under which pixels were treated as background noise, was set to 10. At least 10 individual cells and a minimum of 200 signals were considered for every experiment.

Quantification of Intrinsic FM4-64 Signals in *Arabidopsis* Protoplasts

FM4-64 uptake assays in the absence or presence of GFP-Hub1 in *Arabidopsis* protoplasts were performed in double blind experiments. For every condition, 20 individual pictures were captured 30 min after the addition of FM4-64 (2 μM final concentration). All intracellular FM4-64 signals were considered as intrinsic signals. Standard errors were calculated using Excel (Microsoft).

High-Pressure Freezing and IEM

Four- to five-day-old *Arabidopsis* root tips were cut from the seedling, submerged in 140 mM Suc, 7 mM trehalose, and 7 mM Tris buffer, pH 6.6, transferred into planchettes (Wohlwend; type 241 and 242), and frozen in a high-pressure freezer (HPM010; Bal-Tec). Freeze substitution was performed in a Leica EM AFS2 freeze substitution unit (Leica) in dry acetone supplemented with 0.4% uranyl acetate at −85°C for 16 h before gradually warming up to −50°C over a 5-h period. After washing with 100% ethanol for 60 min, the roots were infiltrated and embedded in Lowicryl HM20 at −50°C (intermediate steps of 30, 50, and 75% HM20 in ethanol, 1 h each) and polymerized for 3 d with UV light in the freeze substitution apparatus. Ultrathin sections were cut on a Leica Ultracut S and incubated with antibodies against BP80 (1:50; Niemes et al., 2010b) or RFP (1:20; Clontech; Living Colors DsRed polyclonal rabbit antibodies), followed by incubation with 10-nm gold-coupled secondary antibodies (BioCell GAR10) at a dilution of 1:50 in PBS supplemented with 1% BSA. Double immunogold labeling on the *Arabidopsis* SYP61-CFP line was performed using monoclonal mouse GFP antibodies (Roche) diluted 1:25, followed by incubation with 5-nm gold-coupled secondary antibodies (BioCell GAR10). Subsequently, immunogold labeling using the polyclonal rabbit VPS28 antibody (1:600) was performed on the same sections, followed by incubation with 15-nm gold-coupled secondary antibodies (BioCell GAR10). For structural analysis, root tips were freeze substituted (72 h, –90°C; 8 h, –60°C; 8 h, –35°C; and 4 h, 0°C) in acetone containing 2% osmium tetroxide, washed at 0°C, and embedded in Spurr's resin. Sections were examined in a JEM1400 transmission electron microscope (JEOL) operating at 80 kV. Micrographs were recorded with a FastScan F214 digital camera (TVIPS).

Chemical Fixation for Electron Microscopy

Arabidopsis seedlings were fixed immersed in 25 mM cacodylate (Caco) buffer, pH 7.2, containing 2% (v/v) glutaraldehyde and 10% (v/v) saturated picric acid at 4°C for 16 h. After four washes of 15 min each in 25 mM Caco buffer, pH 7.2, seedlings were transferred in a secondary fixative containing 2% (w/v) osmium tetroxide and 0.5% (w/v) potassium ferrocyanid in 25 mM Caco buffer, pH 7.2, for 2 h at room temperature. Seedlings were washed twice in 25 mM Caco, pH 7.2, and twice in distilled water before transferring to 2% (w/v) aqueous uranyl acetate for 16 h at 4°C. After four washes in water, seedlings were dehydrated in acetone 30, 50, 70, and 90% in water and twice in acetone 100% for 15 min each at room temperature. Root tips were cut from the seedlings and submerged in 25, 50, and 75% Spurr's resin in acetone and than in 100% Spurr's resin for 45 min each at room temperature, and finally transferred in fresh Spurr's resin 100% at 4°C for 16 h. Samples were transferred in fresh Spurr's resin 100% for 4 h and then placed in the oven at 60°C for polymerization.

Quantification of MVBs in Root Cells

The quantification was conducted on ultrathin sections of 5-d-old *Arabidopsis* root tips using a JEM 1400 transmission electron microscope (JEOL) operating at 80 kV. The root tips were sectioned longitudinally, close to the central axis. MVBs were counted in all the cell types of the meristematic zone. Standard deviations were calculated using Excel (Microsoft).

Quantitative Analysis of IEM

The quantitative analysis was conducted on ultrathin sections previously immunolabeled at the optimal dilution of the respective antibodies for BP80, mRFP-ARA7, and VPS28. The sections were analyzed and

every Golgi apparatus and/or every endosomal compartment encountered during the screening of cells that did not present folding, scratches, or any source of unspecific labeling was taken into consideration. For the labeling density parameter, the area of the single compartments was calculated using the image processing program ImageJ (http://rsbweb.nih.gov/ij). Standard deviations were calculated using Excel (Microsoft).

Accession Numbers

Sequence data from this article can be found in the Arabidopsis Genome Initiative or GenBank/EMBL databases under the following accession numbers: VPS28, AT4G21560; VPS22, At4g27040; VPS2, At2g06530; VHA-a1, At2g28520; ARA6, At3g54840; ARA7, At4g19640; SYP61, At1g28490; VSR2, At2g30290; ANNAT3, At2g38760; NtAnx1, GI:3219615; and NtAnx3, GI:4580919.

Supplemental Data

The following materials are available in the online version of this article.

Supplemental Figure 1. ConcA Affects the Distribution of Marker Proteins for TGN/EE and MVB/LE.

Supplemental Figure 2. Differential Localization of the ESCRT Components VPS22-GFP and VPS2-GFP.

Supplemental Figure 3. VPS22-GFP and VPS2-GFP Do Not Colocalize with Golgi Markers but VPS2 Is Found at the MVB/LE.

Supplemental Figure 4. Time Course to Study the Temporal Distribution of YFP-SYP61 and mRFP-VSR2 as TGN/EE and MVB/LE Markers.

Supplemental Figure 5. Expression of VPS2-DN Affects the Distribution of Markers for the TGN/EE and MVB/LE.

Supplemental Figure 6. RNAi-SNX2a Prevents Arrival of mRFP-VSR2 at the MVB/LE but Does Not Affect Vacuolar Transport.

Supplemental Figure 7. Relationship, Expression, and Knockdown of Plant Annexins.

Supplemental Table 1. Primers Used for Cloning.

ACKNOWLEDGMENTS

We thank Liwen Jiang (Chinese University of Hong Kong, Hong Kong) for kindly providing mRFP-VSR2 encoding plasmids and BP80 antisera and Natasha Raikhel (University of California, Riverside, CA) for kindly providing the SYP61-CFP *Arabidopsis* line. We thank York-Dieter Stierhof (Center for Plant Molecular Biology, University of Tübingen) for helpful discussions on EM. We thank Joachim Kilian and Kenneth W. Berendzen (Center for Plant Molecular Biology, Cytometric Unit, University of Tübingen) for fluorescence-assisted cell sorting of protoplasts and Barbara Jesenofsky, Beate Schöfer, and Steffi Gold (Centre for Organismal Studies) for technical help. The financial support of the Deutsche Forschungsgemeinschaft (PI 769/1-1 and RO 440/14-1) is gratefully acknowledged.

AUTHOR CONTRIBUTIONS

D.S., C.V., D.G.R., P.P., and K.S. designed and analyzed the experiments. D.S., C.V., F. Krüger, F. Künzl, S.S., J.B., and S.H. performed the experiments. L.F. contributed unpublished material. D.S., C.V., D.G.R., P.P., and K.S. wrote the article.

Received April 30, 2011; revised August 19, 2011; accepted August 31, 2011; published September 20, 2011.

REFERENCES

Abramoff, M.D., Magelhaes, P.J., and Ram, S.J. (2004). Image processing with ImageJ. Biophotonics International **11:** 36–42.

Aniento, F., Papavassiliou, A.G., Knecht, E., and Roche, E. (1996). Selective uptake and degradation of c-Fos and v-Fos by rat liver lysosomes. FEBS Lett. **390:** 47–52.

Babst, M., Katzmann, D.J., Estepa-Sabal, E.J., Meerloo, T., and Emr, S.D. (2002a). Escrt-III: An endosome-associated heterooligomeric protein complex required for mvb sorting. Dev. Cell **3:** 271–282.

Babst, M., Katzmann, D.J., Snyder, W.B., Wendland, B., and Emr, S.D. (2002b). Endosome-associated complex, ESCRT-II, recruits transport machinery for protein sorting at the multivesicular body. Dev. Cell **3:** 283–289.

Bilodeau, P.S., Urbanowski, J.L., Winistorfer, S.C., and Piper, R.C. (2002). The Vps27p Hse1p complex binds ubiquitin and mediates endosomal protein sorting. Nat. Cell Biol. **4:** 534–539.

Bonifacino, J.S., and Hurley, J.H. (2008). Retromer. Curr. Opin. Cell Biol. **20:** 427–436.

Braulke, T., and Bonifacino, J.S. (2009). Sorting of lysosomal proteins. Biochim. Biophys. Acta **1793:** 605–614.

Bubeck, J., Scheuring, D., Hummel, E., Langhans, M., Viotti, C., Foresti, O., Denecke, J., Banfield, D.K., and Robinson, D.G. (2008). The syntaxins SYP31 and SYP81 control ER-Golgi trafficking in the plant secretory pathway. Traffic **9:** 1629–1652.

Carlton, J.G., Bujny, M.V., Peter, B.J., Oorschot, V.M., Rutherford, A., Arkell, R.S., Klumperman, J., McMahon, H.T., and Cullen, P.J. (2005). Sorting nexin-2 is associated with tubular elements of the early endosome, but is not essential for retromer-mediated endosome-to-TGN transport. J. Cell Sci. **118:** 4527–4539.

Casadaban, M.J., and Cohen, S.N. (1980). Analysis of gene control signals by DNA fusion and cloning in *Escherichia coli*. J. Mol. Biol. **138:** 179–207.

Chow, C.M., Neto, H., Foucart, C., and Moore, I. (2008). Rab-A2 and Rab-A3 GTPases define a trans-golgi endosomal membrane domain in *Arabidopsis* that contributes substantially to the cell plate. Plant Cell **20:** 101–123.

Clague, M.J. (2002). Membrane transport: A coat for ubiquitin. Curr. Biol. **12:** R529–R531.

Clough, S.J., and Bent, A.F. (1998). Floral dip: A simplified method for Agrobacterium-mediated transformation of *Arabidopsis thaliana*. Plant J. **16:** 735–743.

daSilva, L.L., Taylor, J.P., Hadlington, J.L., Hanton, S.L., Snowden, C.J., Fox, S.J., Foresti, O., Brandizzi, F., and Denecke, J. (2005). Receptor salvage from the prevacuolar compartment is essential for efficient vacuolar protein targeting. Plant Cell **17:** 132–148.

Dettmer, J., Hong-Hermesdorf, A., Stierhof, Y.D., and Schumacher, K. (2006). Vacuolar H+-ATPase activity is required for endocytic and secretory trafficking in *Arabidopsis*. Plant Cell **18:** 715–730.

Dhonukshe, P., Aniento, F., Hwang, I., Robinson, D.G., Mravec, J., Stierhof, Y.D., and Friml, J. (2007). Clathrin-mediated constitutive endocytosis of PIN auxin efflux carriers in Arabidopsis. Curr. Biol. **17:** 520–527.

Doyotte, A., Russell, M.R., Hopkins, C.R., and Woodman, P.G. (2005). Depletion of TSG101 forms a mammalian "Class E" compartment: A multicisternal early endosome with multiple sorting defects. J. Cell Sci. **118:** 3003–3017.

Foresti, O., Gershlick, D.C., Bottanelli, F., Hummel, E., Hawes, C., and Denecke, J. (2010). A recycling-defective vacuolar sorting receptor reveals an intermediate compartment situated between prevacuoles and vacuoles in tobacco. Plant Cell **22:** 3992–4008.

Frangioni, J.V., and Neel, B.G. (1993). Solubilization and purification of

enzymatically active glutathione S-transferase (pGEX) fusion proteins. Anal. Biochem. **210:** 179–187.

French, A.P., Mills, S., Swarup, R., Bennett, M.J., and Pridmore, T.P. (2008). Colocalization of fluorescent markers in confocal microscope images of plant cells. Nat. Protoc. **3:** 619–628.

Futter, C.E., and White, I.J. (2007). Annexins and endocytosis. Traffic **8:** 951–958.

Gabriely, G., Kama, R., and Gerst, J.E. (2007). Involvement of specific COPI subunits in protein sorting from the late endosome to the vacuole in yeast. Mol. Cell. Biol. **27:** 526–540.

Geldner, N., Hyman, D.L., Wang, X., Schumacher, K., and Chory, J. (2007). Endosomal signaling of plant steroid receptor kinase BRI1. Genes Dev. **21:** 1598–1602.

Griffiths, G., and Gruenberg, J. (1991). The arguments for pre-existing early and late endosomes. Trends Cell Biol. **1:** 5–9.

Haas, T.J., Sliwinski, M.K., Martínez, D.E., Preuss, M., Ebine, K., Ueda, T., Nielsen, E., Odorizzi, G., and Otegui, M.S. (2007). The *Arabidopsis* AAA ATPase SKD1 is involved in multivesicular endosome function and interacts with its positive regulator LYST-INTERACTING PROTEIN5. Plant Cell **19:** 1295–1312.

Hillmer, S., Freundt, H., and Robinson, D.G. (1988). The partially coated reticulum and its relationship to the Golgi apparatus in higher plant cells. Eur. J. Cell Biol. **47:** 206–212.

Hunter, P.R., Craddock, C.P., Di Benedetto, S., Roberts, L.M., and Frigerio, L. (2007). Fluorescent reporter proteins for the tonoplast and the vacuolar lumen identify a single vacuolar compartment in Arabidopsis cells. Plant Physiol. **145:** 1371–1382.

Hurley, J.H., and Hanson, P.I. (2010). Membrane budding and scission by the ESCRT machinery: It's all in the neck. Nat. Rev. Mol. Cell Biol. **11:** 556–566.

Hurley, J.H., and Yang, D. (2008). MIT domainia. Dev. Cell **14:** 6–8.

Jovic, M., Sharma, M., Rahajeng, J., and Caplan, S. (2010). The early endosome: A busy sorting station for proteins at the crossroads. Histol. Histopathol. **25:** 99–112.

Kang, B.H., Nielsen, E., Preuss, M.L., Mastronarde, D., and Staehelin, L.A. (2011). Electron tomography of RabA4b- and PI-4Kβ1-labeled trans Golgi network compartments in Arabidopsis. Traffic **12:** 313–329.

Kang, B.H., and Staehelin, L.A. (2008). ER-to-Golgi transport by COPII vesicles in Arabidopsis involves a ribosome-excluding scaffold that is transferred with the vesicles to the Golgi matrix. Protoplasma **234:** 51–64.

Katzmann, D.J., Babst, M., and Emr, S.D. (2001). Ubiquitin-dependent sorting into the multivesicular body pathway requires the function of a conserved endosomal protein sorting complex, ESCRT-I. Cell **106:** 145–155.

Kim, H., Kang, H., Jang, M., Chang, J.H., Miao, Y., Jiang, L., and Hwang, I. (2010). Homomeric interaction of AtVSR1 is essential for its function as a vacuolar sorting receptor. Plant Physiol. **154:** 134–148.

Kirsch, T., Paris, N., Butler, J.M., Beevers, L., and Rogers, J.C. (1994). Purification and initial characterization of a potential plant vacuolar targeting receptor. Proc. Natl. Acad. Sci. USA **91:** 3403–3407.

Lam, S.K., Siu, C.L., Hillmer, S., Jang, S., An, G., Robinson, D.G., and Jiang, L. (2007). Rice SCAMP1 defines clathrin-coated, trans-golgi-located tubular-vesicular structures as an early endosome in tobacco BY-2 cells. Plant Cell **19:** 296–319.

Laohavisit, A., and Davies, J.M. (2011). Annexins. New Phytol. **189:** 40–53.

Leung, K.F., Dacks, J.B., and Field, M.C. (2008). Evolution of the multivesicular body ESCRT machinery; retention across the eukaryotic lineage. Traffic **9:** 1698–1716.

Liu, S.H., Marks, M.S., and Brodsky, F.M. (1998). A dominant-negative clathrin mutant differentially affects trafficking of molecules with distinct sorting motifs in the class II major histocompatibility complex (MHC) pathway. J. Cell Biol. **140:** 1023–1037.

Liu, S.H., Wong, M.L., Craik, C.S., and Brodsky, F.M. (1995). Regulation of clathrin assembly and trimerization defined using recombinant triskelion hubs. Cell **83:** 257–267.

Luzio, J.P., Piper, S.C., Bowers, K., Parkinson, M.D., Lehner, P.J., and Bright, N.A. (2009). ESCRT proteins and the regulation of endocytic delivery to lysosomes. Biochem. Soc. Trans. **37:** 178–180.

Mari, M., Bujny, M.V., Zeuschner, D., Geerts, W.J., Griffith, J., Petersen, C.M., Cullen, P.J., Klumperman, J., and Geuze, H.J. (2008). SNX1 defines an early endosomal recycling exit for sortilin and mannose 6-phosphate receptors. Traffic **9:** 380–393.

Matsuoka, K., Higuchi, T., Maeshima, M., and Nakamura, K. (1997). A vacuolar-type H+-ATPase in a nonvacuolar organelle is required for the sorting of soluble vacuolar protein precursors in tobacco cells. Plant Cell **9:** 533–546.

Mayran, N., Parton, R.G., and Gruenberg, J. (2003). Annexin II regulates multivesicular endosome biogenesis in the degradation pathway of animal cells. EMBO J. **22:** 3242–3253.

Mellman, I., Fuchs, R., and Helenius, A. (1986). Acidification of the endocytic and exocytic pathways. Annu. Rev. Biochem. **55:** 663–700.

Miao, Y., and Jiang, L. (2007). Transient expression of fluorescent fusion proteins in protoplasts of suspension cultured cells. Nat. Protoc. **2:** 2348–2353.

Miao, Y., Li, K.Y., Li, H.Y., Yao, X., and Jiang, L. (2008). The vacuolar transport of aleurain-GFP and 2S albumin-GFP fusions is mediated by the same pre-vacuolar compartments in tobacco BY-2 and Arabidopsis suspension cultured cells. Plant J. **56:** 824–839.

Miao, Y., Yan, P.K., Kim, H., Hwang, I., and Jiang, L. (2006). Localization of green fluorescent protein fusions with the seven Arabidopsis vacuolar sorting receptors to prevacuolar compartments in tobacco BY-2 cells. Plant Physiol. **142:** 945–962.

Morel, E., and Gruenberg, J. (2009). Annexin A2 binding to endosomes and functions in endosomal transport are regulated by tyrosine 23 phosphorylation. J. Biol. Chem. **284:** 1604–1611.

Murk, J.L., Humbel, B.M., Ziese, U., Griffith, J.M., Posthuma, G., Slot, J.W., Koster, A.J., Verkleij, A.J., Geuze, H.J., and Kleijmeer, M.J. (2003). Endosomal compartmentalization in three dimensions: implications for membrane fusion. Proc. Natl. Acad. Sci. USA **100:** 13332–13337.

Nebenführ, A., Gallagher, L.A., Dunahay, T.G., Frohlick, J.A., Mazurkiewicz, A.M., Meehl, J.B., and Staehelin, L.A. (1999). Stop-and-go movements of plant Golgi stacks are mediated by the acto-myosin system. Plant Physiol. **121:** 1127–1142.

Negrutiu, I., Shillito, R., Potrykus, L., Biasini, G., and Sala, F. (1987). Hybrid genes in the analysis of transformation conditions. Plant Mol. Biol. **8:** 363–373.

Nickerson, D.P., West, M., Henry, R., and Odorizzi, G. (2010). Regulators of Vps4 ATPase activity at endosomes differentially influence the size and rate of formation of intralumenal vesicles. Mol. Biol. Cell **21:** 1023–1032.

Niemes, S., Labs, M., Scheuring, D., Krueger, F., Langhans, M., Jesenofsky, B., Robinson, D.G., and Pimpl, P. (2010a). Sorting of plant vacuolar proteins is initiated in the ER. Plant J. **62:** 601–614.

Niemes, S., Langhans, M., Viotti, C., Scheuring, D., San Wan Yan, M., Jiang, L., Hillmer, S., Robinson, D.G., and Pimpl, P. (2010b). Retromer recycles vacuolar sorting receptors from the trans-Golgi network. Plant J. **61:** 107–121.

Obita, T., Saksena, S., Ghazi-Tabatabai, S., Gill, D.J., Perisic, O., Emr, S.D., and Williams, R.L. (2007). Structural basis for selective recognition of ESCRT-III by the AAA ATPase Vps4. Nature **449:** 735–739.

Otegui, M.S., and Spitzer, C. (2008). Endosomal functions in plants. Traffic **9:** 1589–1598.

Paris, N., Rogers, S.W., Jiang, L., Kirsch, T., Beevers, L., Phillips, T.E., and Rogers, J.C. (1997). Molecular cloning and further characterization of a probable plant vacuolar sorting receptor. Plant Physiol. **115:** 29–39.

Peden, A.A., Oorschot, V., Hesser, B.A., Austin, C.D., Scheller, R.H., and Klumperman, J. (2004). Localization of the AP-3 adaptor complex defines a novel endosomal exit site for lysosomal membrane proteins. J. Cell Biol. **164:** 1065–1076.

Pesacreta, T.C., and Lucas, W.J. (1984). Plasma membrane coat and a coated vesicle-associated reticulum of membranes: Their structure and possible interrelationship in Chara corallina. J. Cell Biol. **98:** 1537–1545.

Phillipson, B.A., Pimpl, P., daSilva, L.L., Crofts, A.J., Taylor, J.P., Movafeghi, A., Robinson, D.G., and Denecke, J. (2001). Secretory bulk flow of soluble proteins is efficient and COPII dependent. Plant Cell **13:** 2005–2020.

Pimpl, P., Hanton, S.L., Taylor, J.P., Pinto-daSilva, L.L., and Denecke, J. (2003). The GTPase ARF1p controls the sequence-specific vacuolar sorting route to the lytic vacuole. Plant Cell **15:** 1242–1256.

Pimpl, P., Taylor, J.P., Snowden, C., Hillmer, S., Robinson, D.G., and Denecke, J. (2006). Golgi-mediated vacuolar sorting of the endoplasmic reticulum chaperone BiP may play an active role in quality control within the secretory pathway. Plant Cell **18:** 198–211.

Piper, R.C., and Katzmann, D.J. (2007). Biogenesis and function of multivesicular bodies. Annu. Rev. Cell Dev. Biol. **23:** 519–547.

Polo, S., Sigismund, S., Faretta, M., Guidi, M., Capua, M.R., Bossi, G., Chen, H., De Camilli, P., and Di Fiore, P.P. (2002). A single motif responsible for ubiquitin recognition and monoubiquitination in endocytic proteins. Nature **416:** 451–455.

Poteryaev, D., Datta, S., Ackema, K., Zerial, M., and Spang, A. (2010). Identification of the switch in early-to-late endosome transition. Cell **141:** 497–508.

Raymond, C.K., Howald-Stevenson, I., Vater, C.A., and Stevens, T.H. (1992). Morphological classification of the yeast vacuolar protein sorting mutants: evidence for a prevacuolar compartment in class E vps mutants. Mol. Biol. Cell **3:** 1389–1402.

Razi, M., Chan, E.Y., and Tooze, S.A. (2009). Early endosomes and endosomal coatomer are required for autophagy. J. Cell Biol. **185:** 305–321.

Reichardt, I., Stierhof, Y.D., Mayer, U., Richter, S., Schwarz, H., Schumacher, K., and Jürgens, G. (2007). Plant cytokinesis requires de novo secretory trafficking but not endocytosis. Curr. Biol. **17:** 2047–2053.

Rink, J., Ghigo, E., Kalaidzidis, Y., and Zerial, M. (2005). Rab conversion as a mechanism of progression from early to late endosomes. Cell **122:** 735–749.

Ritzenthaler, C., Nebenführ, A., Movafeghi, A., Stussi-Garaud, C., Behnia, L., Pimpl, P., Staehelin, L.A., and Robinson, D.G. (2002). Reevaluation of the effects of brefeldin A on plant cells using tobacco Bright Yellow 2 cells expressing Golgi-targeted green fluorescent protein and COPI antisera. Plant Cell **14:** 237–261.

Robert, S., Chary, S.N., Drakakaki, G., Li, S., Yang, Z., Raikhel, N.V., and Hicks, G.R. (2008). Endosidin1 defines a compartment involved in endocytosis of the brassinosteroid receptor BRI1 and the auxin transporters PIN2 and AUX1. Proc. Natl. Acad. Sci. USA **105:** 8464–8469.

Robinson, D.G., Jiang, L., and Schumacher, K. (2008). The endosomal system of plants: Charting new and familiar territories. Plant Physiol. **147:** 1482–1492.

Sachse, M., Urbé, S., Oorschot, V., Strous, G.J., and Klumperman, J. (2002). Bilayered clathrin coats on endosomal vacuoles are involved in protein sorting toward lysosomes. Mol. Biol. Cell **13:** 1313–1328.

Saint-Jean, B., Seveno-Carpentier, E., Alcon, C., Neuhaus, J.M., and Paris, N. (2010). The cytosolic tail dipeptide Ile-Met of the pea receptor BP80 is required for recycling from the prevacuole and for endocytosis. Plant Cell **22:** 2825–2837.

Schellmann, S., and Pimpl, P. (2009). Coats of endosomal protein sorting: Retromer and ESCRT. Curr. Opin. Plant Biol. **12:** 670–676.

Shahriari, M., Keshavaiah, C., Scheuring, D., Sabovljevic, A., Pimpl, P., Häusler, R.E., Hülskamp, M., and Schellmann, S. (2010). The AAA-type ATPase AtSKD1 contributes to vacuolar maintenance of *Arabidopsis thaliana*. Plant J. **64:** 71–85.

Shahriari, M., Richter, K., Keshavaiah, C., Sabovljevic, A., Huelskamp, M., and Schellmann, S. (2011). The Arabidopsis ESCRT protein-protein interaction network. Plant Mol. Biol. **76:** 85–96.

Spitzer, C., Reyes, F.C., Buono, R., Sliwinski, M.K., Haas, T.J., and Otegui, M.S. (2009). The ESCRT-related CHMP1A and B proteins mediate multivesicular body sorting of auxin carriers in *Arabidopsis* and are required for plant development. Plant Cell **21:** 749–766.

Stierhof, Y.D., and El Kasmi, F. (2010). Strategies to improve the antigenicity, ultrastructure preservation and visibility of trafficking compartments in Arabidopsis tissue. Eur. J. Cell Biol. **89:** 285–297.

Stoorvogel, W., Oorschot, V., and Geuze, H.J. (1996). A novel class of clathrin-coated vesicles budding from endosomes. J. Cell Biol. **132:** 21–33.

Tanchak, M.A., Rennie, P.J., and Fowke, L.C. (1988). Ultrastrucure of the partially coated reticulum and dictyosomes during endocytosis by soybean protoplasts. Planta **175:** 433–441.

Taub, N., Teis, D., Ebner, H.L., Hess, M.W., and Huber, L.A. (2007). Late endosomal traffic of the epidermal growth factor receptor ensures spatial and temporal fidelity of mitogen-activated protein kinase signaling. Mol. Biol. Cell **18:** 4698–4710.

Tooze, J., and Hollinshead, M. (1991). Tubular early endosomal networks in AtT20 and other cells. J. Cell Biol. **115:** 635–653.

Toyooka, K., Goto, Y., Asatsuma, S., Koizumi, M., Mitsui, T., and Matsuoka, K. (2009). A mobile secretory vesicle cluster involved in mass transport from the Golgi to the plant cell exterior. Plant Cell **21:** 1212–1229.

Tse, Y.C., Mo, B., Hillmer, S., Zhao, M., Lo, S.W., Robinson, D.G., and Jiang, L. (2004). Identification of multivesicular bodies as prevacuolar compartments in *Nicotiana tabacum* BY-2 cells. Plant Cell **16:** 672–693.

Ueda, T., Uemura, T., Sato, M.H., and Nakano, A. (2004). Functional differentiation of endosomes in Arabidopsis cells. Plant J. **40:** 783–789.

Uemura, T., Ueda, T., Ohniwa, R.L., Nakano, A., Takeyasu, K., and Sato, M.H. (2004). Systematic analysis of SNARE molecules in Arabidopsis: Dissection of the post-Golgi network in plant cells. Cell Struct. Funct. **29:** 49–65.

van Dam, E.M., and Stoorvogel, W. (2002). Dynamin-dependent transferrin receptor recycling by endosome-derived clathrin-coated vesicles. Mol. Biol. Cell **13:** 169–182.

van Meel, E., and Klumperman, J. (2008). Imaging and imagination: Understanding the endo-lysosomal system. Histochem. Cell Biol. **129:** 253–266.

van Weering, J.R., Verkade, P., and Cullen, P.J. (2010). SNX-BAR proteins in phosphoinositide-mediated, tubular-based endosomal sorting. Semin. Cell Dev. Biol. **21:** 371–380.

Viotti, C., et al. (2010). Endocytic and secretory traffic in *Arabidopsis* merge in the trans-Golgi network/early endosome, an independent and highly dynamic organelle. Plant Cell **22:** 1344–1357.

Wang, H., Zhuang, X., Hillmer, S., Robinson, D.G., and Jiang, L. (March 23, 2011). Vacuolar sorting receptor (VSR) proteins reach the plasma membrane in germinating pollen tubes. Mol. Plant http://dx.doi.org/10.1093/mp/ssr011.

Winter, V., and Hauser, M.T. (2006). Exploring the ESCRTing machinery in eukaryotes. Trends Plant Sci. **11:** 115–123.

Wollert, T., and Hurley, J.H. (2010). Molecular mechanism of multivesicular body biogenesis by ESCRT complexes. Nature **464:** 864–869.

Yoo, S.Y., Bomblies, K., Yoo, S.K., Yang, J.W., Choi, M.S., Lee, J.S., Weigel, D., and Ahn, J.H. (2005). The 35S promoter used in a selectable marker gene of a plant transformation vector affects the expression of the transgene. Planta **221:** 523–530.

Yoshimori, T., Yamagata, F., Yamamoto, A., Mizushima, N., Kabeya, Y., Nara, A., Miwako, I., Ohashi, M., Ohsumi, M., and Ohsumi, Y. (2000). The mouse SKD1, a homologue of yeast Vps4p, is required for normal endosomal trafficking and morphology in mammalian cells. Mol. Biol. Cell **11:** 747–763.

Zouhar, J., Muñoz, A., and Rojo, E. (2010). Functional specialization within the vacuolar sorting receptor family: VSR1, VSR3 and VSR4 sort vacuolar storage cargo in seeds and vegetative tissues. Plant J. **64:** 577–588.